CHAPTER – 4

RESULT

4. RESULT

OBJECTIVE 1. Study of phytochemical content, antioxidant and anthelmintic activity of *Hypericum japonicum* crude extracts and solvent fractions

4.1. Collection, authentication, and preparation of crude extract and solvent fractions

A plant sample of *Hypericum japonicum* was collected from the Tinali area of Kokrajhar, Assam, a region known for its diverse flora. The sample was authenticated by a taxonomist from the Department of Botany, Bodoland University, and identified as *Hypericum japonicum* Thunb., with the assigned identification number BUBH2000129. Figure 8a shows the plant photograph and preparation of herbarium sheet (Figure 8b). The moisture content of the fresh plant material was analyzed and found to be 84.09 ± 8.99 g/100g wet weight, indicating high water content typical of freshly harvested plant samples. This parameter is critical as it directly influences the drying process, storage stability, and subsequent extraction efficiency. After drying the plant material, crude extraction was performed, yielding 18.43 ± 2.33 g/100g dry powder. This crude extract yield reflects the concentration of extractable compounds, including bioactive phytochemicals, present in the plant material. These results set the foundation for comprehensive phytochemical analysis, and bioactivity assays, ultimately contributing to the validation of the plant's traditional medicinal uses and its potential for pharmaceutical applications.

4.2. Solvent Fractionation

Solvent fractionation is a process used to separate compounds from a crude extract based on their solubility in solvents of varying polarity. This method allows for the selective extraction of bioactive phytochemicals by employing solvents such as hexane, diethyl ether, and ethyl acetate. Each solvent targets specific classes of compounds, with non-polar solvents like hexane extracting lipophilic compounds, moderately polar solvents like diethyl ether extracting intermediate-polarity compounds, and polar solvents like ethyl acetate extracting more polar compounds. For the preparation of solvent fractions, three solvents—hexane (polarity index 0.1), diethyl ether (polarity index 2.8), and ethyl acetate

(polarity index 4.1) —were selected based on their polarity to ensure efficient separation of phytochemicals with varying polarities. A total of 10 g of methanolic crude extract was subjected to fractionation. The solvent fractions obtained were 860 ± 21.07 mg of hexane (Hex) extract, 200 ± 20 mg of diethyl ether (DE) extract, and 750 ± 30 mg of ethyl acetate (EA) extract. The hydro-alcoholic residue was discarded. These fractions represent the differential solubility of phytochemicals in solvents of varying polarity and provide a basis for further phytochemical profiling and bioactivity studies.

(a) **(b)**

Figure 8. Collection and identification of test plant. (a) *Hypericum japonicum* and (b) Herbarium sheet of *Hypericum japonicum*

4.3. Qualitative and quantitative phytochemical analysis

I. Qualitative Phytochemical Analysis

Phytochemical analysis plays a crucial role in understanding the medicinal potential of plants by identifying the bioactive compounds responsible for their pharmacological properties. Secondary metabolites such as alkaloids, flavonoids, phenols, tannins, and saponins are often the basis for both traditional medicine and modern drug development. Analyzing the phytochemical profile of a plant can help researchers uncover its therapeutic potential, validate traditional uses, and provide insights for further pharmacological and

clinical studies. In the present study, qualitative phytochemical analysis was conducted on different plant solvent extracts, and the results are summarized in Table 1, with images shown in Photo Plate 5 and 6. A total of 15 phytochemicals were screened across four different solvent extracts.

Table 1. Qualitative analysis of different solvent extracts of *Hypericum japonicum*

Test	Hex	DE	EA	Met
Alkaloids	+	+	+	+
Tannins	-	+	+	+
Phenolics	-	+	+	+
Quinones	-	+	+	+
Terpenoids	+	+	+	+
Flavonoids	+	+	+	+
Coumarins	+	+	+	+
Anthocyanin	-	-	-	-
Glycosides	-	-	-	-
Anthraquinones	-	+	+	+
Steroids	-	+	+	+
Triterpenoids	+	-	-	-
Carbohydrates	+	+	+	+
Saponins	+	+	+	+
Proteins	+	+	+	+
Phlobatannins	_	_	+	+

'-'indicates absence; '+' indicates presence; Hex- Hexane; DE- Diethyl ether; EA- Ethyl acetate; Met- Methanol

The analysis revealed that all the phytochemicals were present in one or more solvent fractions, except for anthocyanins and glycosides, which were absent in all extracts. The hexane (Hex) extract exhibited limited phytochemical diversity, with most compounds absent or present in very low concentrations. Only alkaloids, flavonoids, coumarins, triterpenoids, carbohydrates, and saponins were detected in trace amounts. In the diethyl ether (DE) extract, tannins, flavonoids, phenols, coumarins, anthocyanins, glycosides, triterpenoids, and phlobatannins were present. The ethyl acetate (EA) extract demonstrated

presence of alkaloids, tannins, phenols, and coumarins, indicating its effectiveness in extracting a variety of bioactive compounds. Finally, the methanolic extract exhibited the presence of quinones, steroids, saponins, and proteins, highlighting methanol as a potent solvent for extracting compounds with significant pharmacological potential. These findings underscore the importance of solvent selection in phytochemical studies and provide valuable insights for the development of natural therapeutic agents from *Hypericum japonicum*.

II. Quantitative Analysis

The solvent fractions of the plant have been studied for their quantitative phytochemical content. Figure 9 shows the standard graph of protein and carbohydrate. For protein estimation, BSA was taken as the standard of protein. A calibration curve was prepared from standard BSA with ($y = 0.0056x - 0.0027$, $R^2 = 0.9994$) as shown in the Figure 9 (a). For carbohydrate assay, glucose was used as a standard. A calibration curve was prepared from standard gallic acid ($0.0132x + 0.0836$, $R^2 = 0.9807$) as shown in Figure 9 (b). Figure 10 shows the standard graph of total phenolic content and total flavonoid content. For TPC, gallic acid was used as standard and a calibration curve was prepared from standard gallic acid ($y = 0.0203x-0.0141$, $R^2 = 0.9997$) as shown in Figure 10 (a). For TFC, Quercetin was used as the standard and a calibration curve was prepared from quercetin ($y = 0.0162x-0.0268$, $R^2 = 0.9999$) as shown in Figure 10 (b).

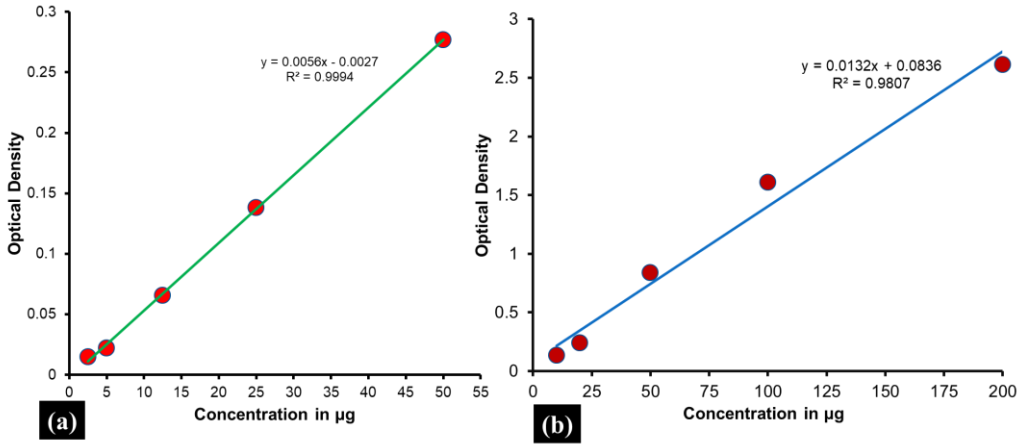

Figure 9. (a) Standard graph of protein (BSA), and (b) Standard graph of carbohydrate (glucose)

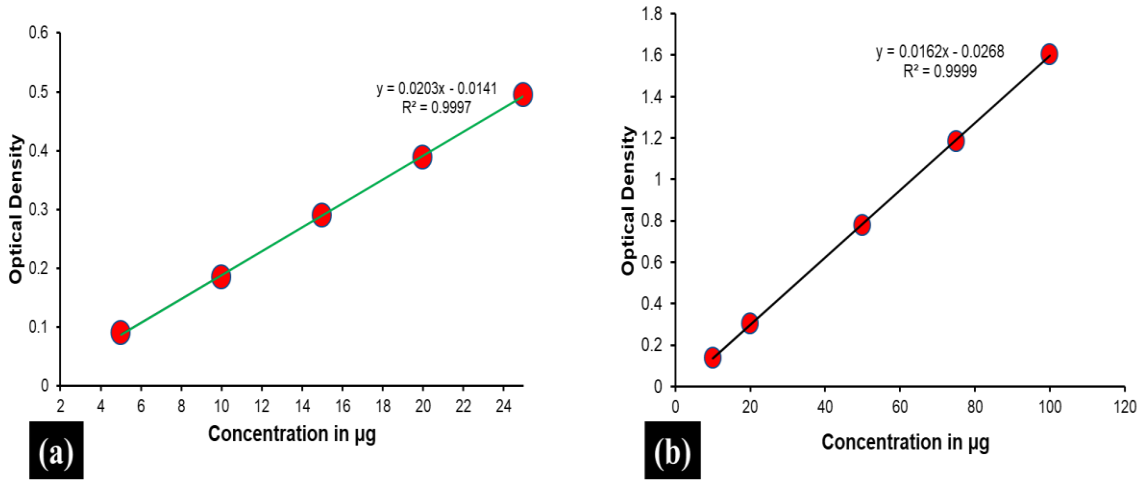

Figure 10. (a) Standard graph of phenolics (gallic acid), and (b) Standard graph of flavonoids (quercetin)

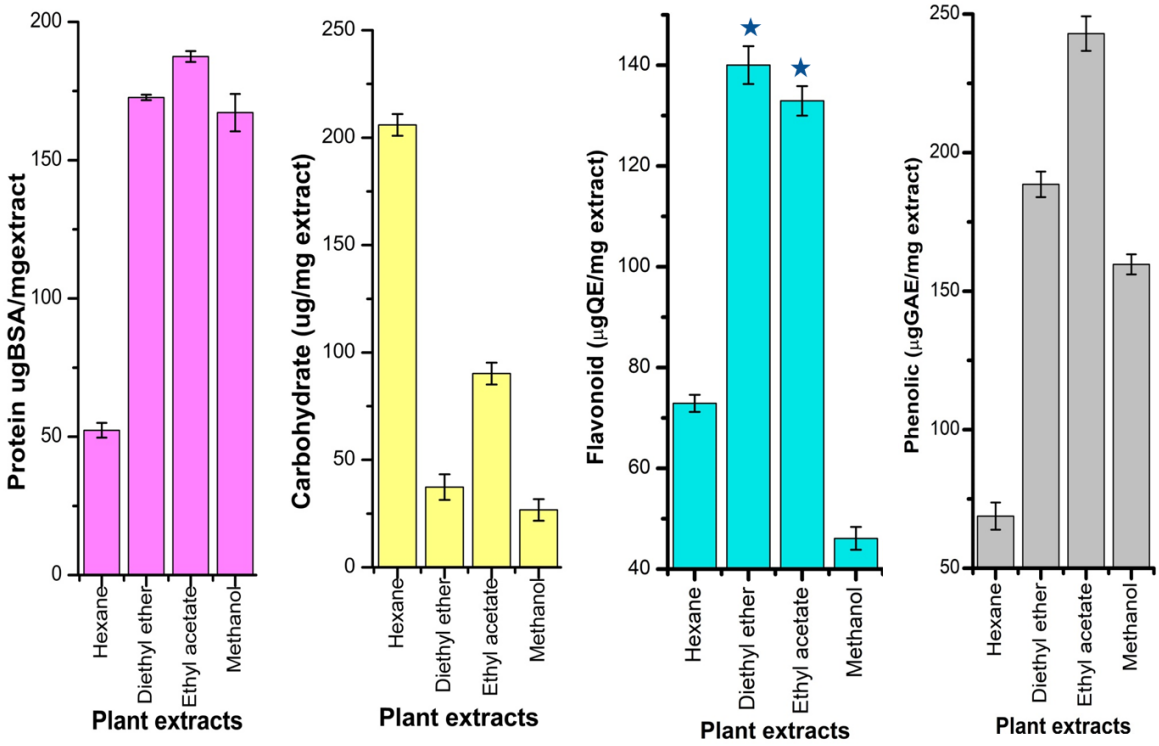

Figure 11. Protein, Carbohydrate, TFC, and TPC of different solvent fractions. Values are expressed as mean ± SD, n=3 (no. of experiments). Protein, carbohydrate and TPC showed mean difference is significant among the four solvent extracts at $P \leq 0.05$ level, except at TFC (diethyl ether and ethyl acetate shown by '*')

Figure 11 shows the protein, carbohydrate, TPC, and TFC of different plant solvent extracts. EA has shown the highest protein content with 187.47 ± 1.96 µg/mg, followed by

DE with 172.67 ± 0.98 µg/mg, Met with 167.20 ± 6.78 µg/mg and hex with 52.33 ± 2.67 µg/mg as shown in Figure 11. For carbohydrate content, highest content has shown in Hex with 205.93 ± 5.07 µg/mg, followed by EA with 90.20 ± 5.07 µg/mg, DE with 37.35 ± 5.97 µg/mg and Met with 26.75 ± 5.01 µg/mg as shown in Figure 11. For the TFC, it has shown highest flavonoid content in DE with 140.02 ± 3.75 µg/mg, followed by EA with 132.93 ± 2.92 µg/mg, Hex with 72.90 ± 1.70 µg/mg and Met with 46.10 ± 2.27 µg/mg as shown in Figure 11. Lastly, for the TPC, it has shown highest phenolic content in EA with 242.96 ± 6.25µg/mg, followed by DE with 188.55 ± 4.62 µg/mg, Met with 159.66 ± 0.63 µg/mg and Hex with 68.82 ± 4.91 µg/mg as shown in Figure 11. Thus, from the above result,we can conclude that among all the four solvent extracts EA has shown highest protein content and TPC, DE has shown highest TFC and Hex has shown highest carbohydrate content.

4.4. Elemental Analysis

For the heavy metal study of *Hypericum japonicum*, five heavy metals were selected. Among them, two were essential elements namely, Copper (Cu) and Zinc (Zn) and three toxic elements- Chromium (Cr), Lead (Pb) and Cadmium (Cd) were analyzed. The heavy metals study for these metals were done because excessive levels of heavy metals can be toxic to plants and pose a risk to human health if consumed.

Table 2. Trace element composition of *Hypericum japonicum*

Heavy metals	Concentration (in ppm)	WHO Threshold limit (in ppm)
Chromium	0.436	2
Copper	0.182	150
Zinc	1.430	100
Cadmium	0.010	0.3
Lead	0.081	10

Table 2 shows the concentrations of the different metals. Our study revealed that the concentrations of the metals were negligible, indicating minimal accumulation. The highest concentration was shown in Zn and the least in Cd. According to WHO (2005), limitations for plant herbal medicines for different heavy metals are Cu- 150 ppm, Cr- 2 ppm, Pb- 10 ppm, Cd- 0.3 ppm, and Zn- 100 ppm. The negligible levels of toxic metals detected in *H. japonicum* suggest that it can be safely consumed for medicinal purposes.

4.5. Antioxidant Study

Antioxidant activity is the ability of a compound to scavenge free radicals and reduce oxidative stress, which is a major contributor to cellular damage and the progression of various diseases. Its pharmacological importance lies in its potential to prevent and manage oxidative stress-related disorders such as cancer, cardiovascular diseases, diabetes, and neurodegenerative conditions like Alzheimer's and Parkinson's disease. Antioxidants also play a critical role in anti-inflammatory and hepatoprotective therapies by modulating oxidative pathways. Furthermore, they enhance the efficacy of drugs by protecting active pharmaceutical ingredients from oxidation and improving stability, making them valuable in drug development and formulation. The antioxidant activity of the solvent fractions has been studied. Figure 12 showing the standard graph of TAC and FRAP. For TAC, ascorbic acid was taken as the standard.

In the present study, the antioxidant activity of the solvent fractions was evaluated using two methods: Total Antioxidant Capacity (TAC) and Ferric Reducing Antioxidant Power (FRAP). For TAC, ascorbic acid was used as the standard, and a calibration curve was prepared with the equation $y=0.0072x+0.0086$, and $R^2=0.9993$, as shown in Figure 12(b). For FRAP, iron (II) sulfate ($FeSO_4$) was used as the standard, with a calibration curve represented by the equation $y=0.269x-0.005$, and $R^2=0.9995$, as depicted in Figure 12(b). Among the four solvent fractions, the diethyl ether (DE) fraction exhibited the highest TAC, with a value of 154.65 ± 1.18 µg/mg, followed by ethyl acetate (EA) with 136.48 ± 1.58 µg/mg, methanol (Met) with 127.97 ± 1.20 µg/mg, and the hexane (Hex) fraction showing the least activity at 115.68 ± 3.88 µg/mg, as shown in Figure 13. In the FRAP assay, EA exhibited the strongest activity with 173.79 ± 6.40 µg/mg, followed by Met with 123.53 ± 4.90 µg/mg, DE with 111.21 ± 3.28 µg/mg, and Hex with the lowest value of 73.2 ± 0.04 µg/mg, as shown in Figure 13.

In the present study, again for antioxidant activity or to see the free radical scavenging activity of various solvent fractions of *Hypericum japonicum* was assessed using several assays to determine their capacity to scavenge free radicals and inhibit oxidative damage. The DPPH (2,2-diphenyl-1-picrylhydrazyl) radical scavenging assay was employed, using gallic acid as the standard antioxidant. The IC_{50} value of gallic acid, which represents the concentration required to inhibit 50% of DPPH radicals, was found to be 3.51 ± 0.01 µg/mL, indicating its potent antioxidant capacity. Among the four solvent

extracts, the ethyl acetate (EA) fraction showed the strongest activity, with an IC_{50} value of 33.29 ± 0.38 µg/mL. This was followed by the methanol (Met) extract (IC_{50} = 59.77 ± 0.30 µg/mL), the diethyl ether (DE) extract (IC_{50} = 78.95 ± 2.82 µg/mL), and the hexane (Hex) extract (IC_{50} = 203.19 ± 1.50 µg/mL), as shown in Figure 14. These results suggest that EA is the most effective solvent in extracting antioxidant compounds capable of neutralizing DPPH radicals, while hexane, being a less polar solvent, showed weaker activity.

Further analysis of the antioxidant potential was conducted using the ABTS (2,2'-azinobis-(3-ethylbenzothiazoline-6-sulfonic acid)) free radical scavenging assay, with gallic acid serving as the standard. Gallic acid demonstrated a strong antioxidant activity with an IC_{50} value of 1.29 ± 0.11 µg/mL. In comparison, the EA extract again showed the strongest free radical scavenging activity, with an IC_{50} value of 14.36 ± 0.75 µg/mL. The DE extract exhibited a moderately strong activity with an IC_{50} of 17.83 ± 0.47 µg/mL, followed by the methanol extract (IC_{50} = 25.94 ± 1.56 µg/mL) and the hexane extract (IC_{50} = 45.16 ± 0.86 µg/mL), as shown in Figure 15. These findings further confirm the strong antioxidant properties of the EA fraction, which efficiently scavenges ABTS radicals, compared to the other extracts. Additionally, the TBARS (Thiobarbituric Acid Reactive Substances) assay, which measures lipid peroxidation inhibition, was performed using ascorbic acid as the standard. The IC_{50} value of ascorbic acid was found to be 28.79 ± 0.07 µg/mL, reflecting its known ability to prevent lipid oxidation. Among the solvent extracts, the EA fraction again demonstrated the strongest activity, with the lowest IC_{50} value of 7.68 ± 0.12 µg/mL, indicating its potent ability to inhibit lipid peroxidation. This was followed by the DE extract (IC_{50} = 8.55 ± 0.39 µg/mL), the methanol extract (IC50 = 42.22 ± 1.02 µg/mL), and the hexane extract, which showed the weakest activity with an IC_{50} value of 267.13 ± 5.27 µg/mL, as shown in Figure 16. The results from all three antioxidant assays (DPPH, ABTS, and TBARS) consistently demonstrate that the ethyl acetate extract possesses the strongest antioxidant activity among the four solvent fractions studied, followed by methanol, diethyl ether, and hexane, respectively. The EA fraction's superior performance across these assays suggests that it contains high concentrations of bioactive compounds with strong free radical scavenging and lipid peroxidation inhibitory properties. These findings highlight the importance of solvent selection in extracting specific antioxidant compounds and suggest that the EA fraction of *Hypericum japonicum* may serve as a valuable source of natural antioxidants for therapeutic applications.

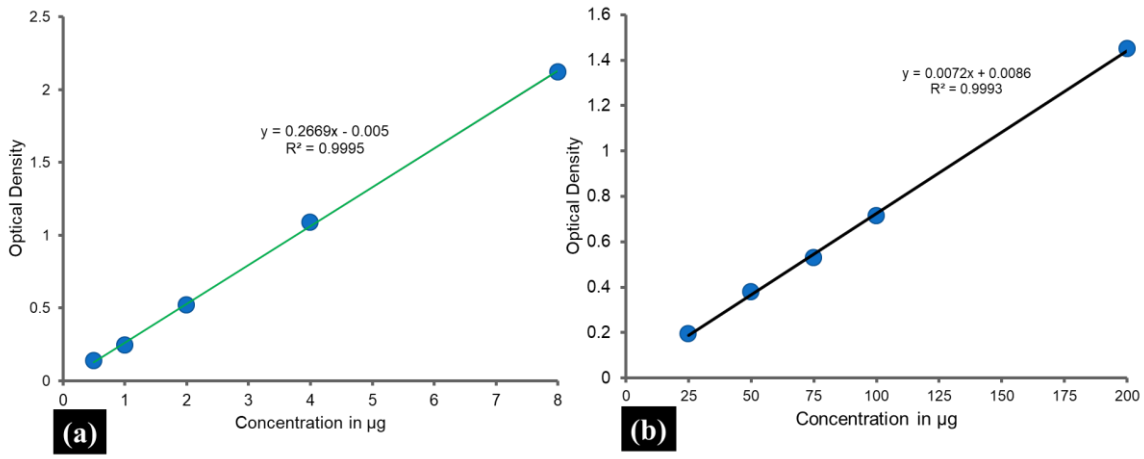

Figure 12. (a) Standard graph of FRAP (ferrous sulphate), and (b) Standard graph of Total antioxidant aassay (ascorbic acid)

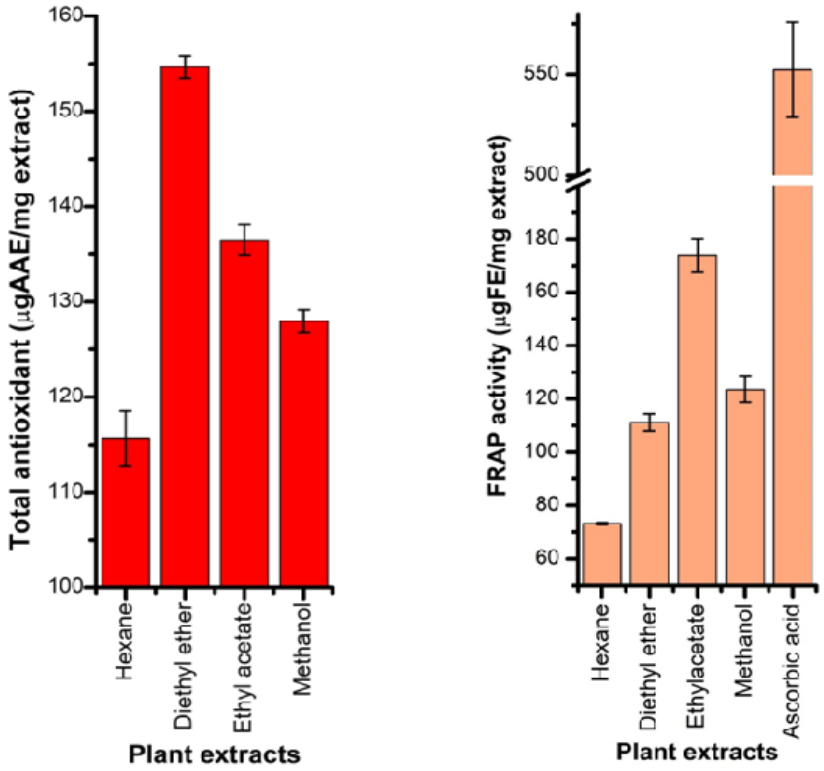

Figure 13. TAC and FRAP activity of different solvent fractions. Values are expressed as mean ± SD, n=3 (no. of experiments). TAC and FRAP showed mean difference is significant among the four solvent extracts at $P \leq 0.05$ level

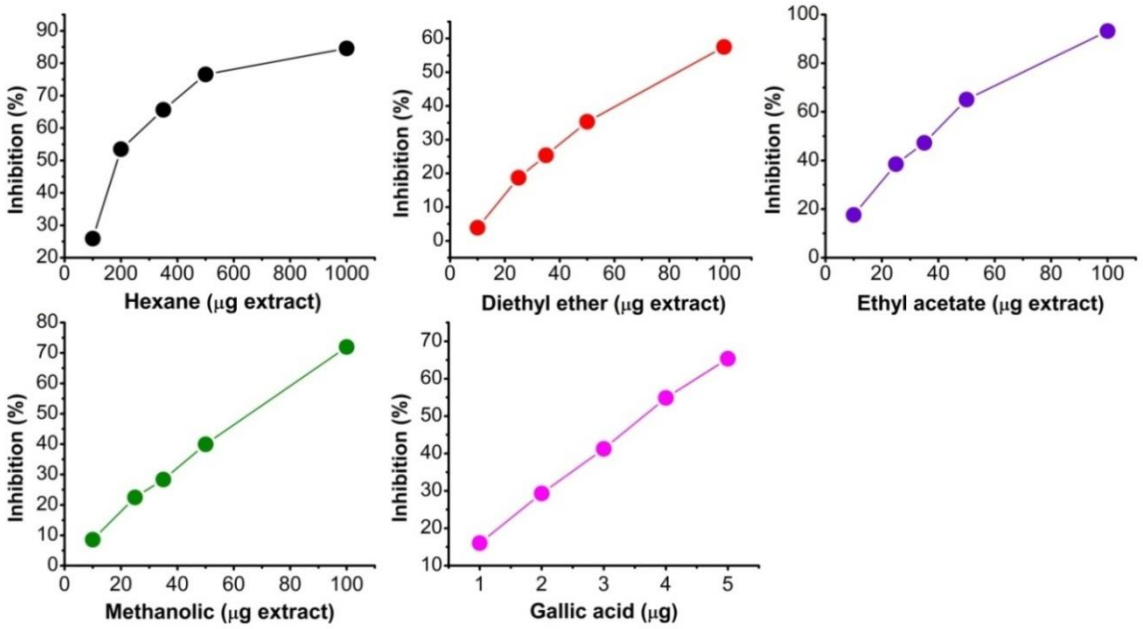

Figure 14. DPPH scavenging activity of different solvent fractions of *Hypericum japonicum.* Values are expressed as mean ± SD, n=3 (no. of experiments). All the solvent fractions showed mean difference is significant among the four solvent extracts at $P \leq 0.05$ level

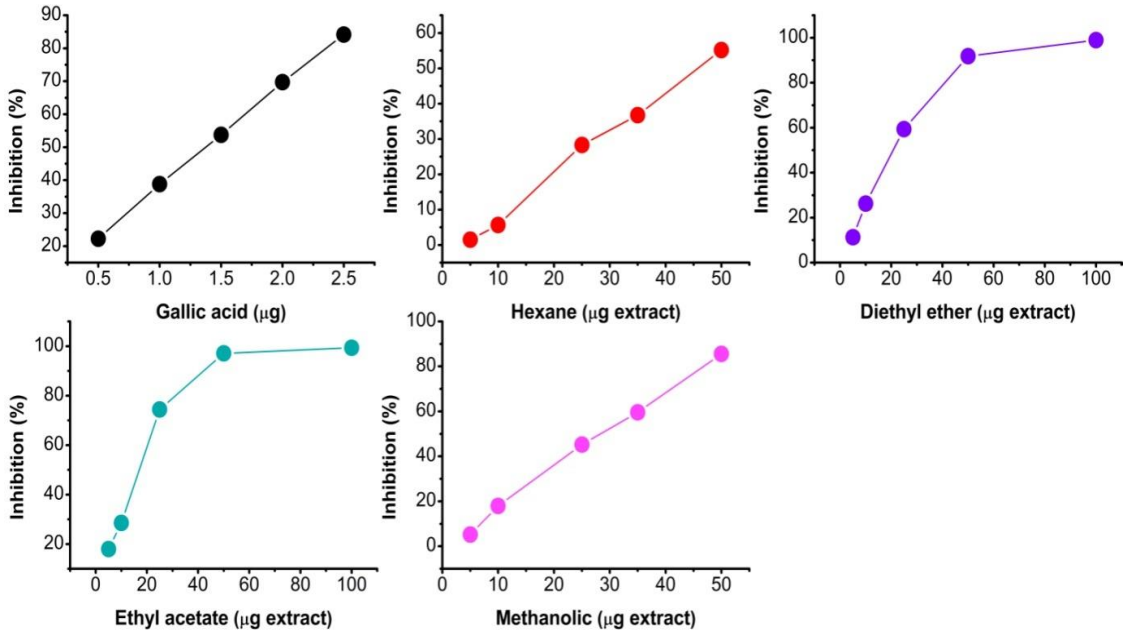

Figure 15. ABTS activity of different solvent fractions of *Hypericum japonicum.* Values are expressed as mean ± SD, n=3 (no. of experiments). All the solvent fractions showed mean difference is significant among the four solvent extracts at $P \leq 0.05$ level

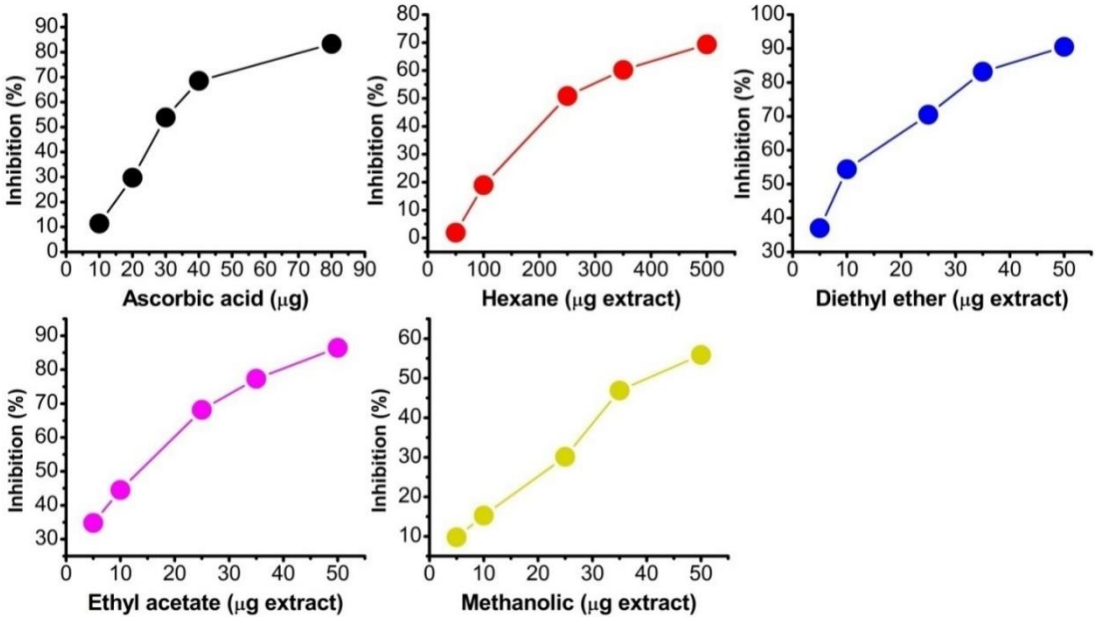

Figure 16 . TBARS activity of different solvent fractions of *Hypericum japonicum*. Values are expressed as mean ± SD, n = 3 (no. of experiments). All the solvent fractions showed mean difference is significant among the four solvent extracts at $P \leq 0.05$ level, except diethyl ether and ethyl acetate

4.6. In-vitro Anthelmintic Study

In the present study, the anthelmintic activity of *Hypericum japonicum* solvent extracts was evaluated on *Paramphistomum spp.*, a parasitic flatworm, using four different solvent extracts: diethyl ether (DE), hexane (Hex), methanol (Met), and ethyl acetate (EA), all at a dose concentration of 5 mg/mL. The study aimed to assess the potential of these extracts in inducing paralysis and death in the parasitic worms, as an indicator of their therapeutic potential in controlling parasitic infections. Among the four solvent extracts, the DE extract exhibited the most potent anthelmintic activity, as indicated by the shortest death time of the worms, which was 3:49 ± 0:21 h:min. This suggests that DE contains bioactive compounds capable of acting more rapidly against *Paramphistomum spp.* compared to the other extracts. The hexane extract also showed significant activity, with a death time of 3:55 ± 0:12 h:min, which was only slightly longer than that of DE. Both the DE and Hex extracts were found to be more effective than the reference drug albendazole, which is commonly used to treat parasitic infections. Albendazole demonstrated a death time of 4:21 ± 0:19 h:min, indicating that DE and Hex extracts of *Hypericum japonicum* might have

comparable or even superior anthelmintic properties to this standard drug. In contrast, the methanol (Met) and ethyl acetate (EA) extracts showed considerably slower activity. The death times for these extracts were much longer, with the Met extract taking 9:54 ± 0:48 h:min and the EA extract taking 14:30 ± 0:24 h:min to kill the worms. These results suggest that the bioactive compounds present in the Met and EA extracts might act more slowly or may require higher concentrations to exhibit similar anthelmintic effects as DE and Hex extracts.

As a control, untreated *Paramphistomum spp.* parasites survived for 73:21 ± 0:33 h:min, confirming that the observed effects were due to the extracts' active components rather than other experimental factors. The differences in the death and paralysis times of the various extracts highlight the potential of *Hypericum japonicum* as a source of natural anthelmintic agents, with DE and Hex extracts demonstrating superior efficacy compared to the reference drug and other extracts. These findings support the idea that *Hypericum japonicum* extracts, particularly those obtained with DE and Hex, contain potent anthelmintic compounds that could be further studied for their potential use in controlling parasitic infections. The detailed data on paralysis and death times for each extract are provided in Table 3, offering a comprehensive overview of the anthelmintic effects observed during the study.

Table 3. Anthelmintic activity of different solvent fractions of *Hypericum japonicum*

Sample	Solvent fractions	Paralysis time (h: min)	Death Time (h: min)
Hypericum japonicum	Hexane	3:49 ± 0:11	3:55 ± 0:12
	Diethyl ether	3:22 ± 0:17	3:49 ± 0:21
	Ethyl acetate	13:20 ± 0:37	14:30 ± 0:24
	Methanol	9:26 ± 0:38	9:54 ± 0:48
Reference chemical	Albendazole	3:50 ± 0:15	4:21 ± 0:19

Control parasite lived up to 73:21+0:33 h:min. Values are expressed as mean ± SD, n = 3 (no. of experiments)

4.7. Histological study of Paramphistomum species treated with diethyl ether plant extract

The tegument of helminth parasites is a specialized and metabolically active outer covering that is critical for their survival and interaction with the host environment. It serves multiple functions, including protection against the host's immune system and digestive enzymes, nutrient absorption, attachment to host tissues, sensory perception, waste removal, and immunomodulation to evade host defenses. Histological studies were conducted to evaluate the effects of treatments on the tegument's structural integrity, using untreated parasites (control), parasites treated with albendazole (a standard anthelmintic drug), and those treated with DE extract. Observations were made at 4X, 20X, and 40X magnifications.

In the control group (figure 17), the tegument appeared smooth, intact, and without any ruptures or irregularities, indicating a healthy, functional outer layer. This smooth and undamaged tegument demonstrates its ability to maintain essential physiological functions in the host environment. However, parasites treated with albendazole (Figure 18) exhibited significant structural damage to the tegument, characterized by clear breakage, roughness, and disruption of the outer layer. These changes suggest a loss of the parasite's protective barrier and functional capacity, rendering it vulnerable to the host’s immune response and leading to its eventual death. Similarly, treatment with DE extract (figure 19) induced extensive damage to the tegument, with roughness and continuous breakage observed in its structure. The disruption of the tegument likely interferes with the parasite's ability to absorb nutrients, excrete waste, and protect itself from the host's defenses, ultimately impairing its survival. These observations indicate that the DE extract, like albendazole, has a profound impact on the integrity of the tegument, making it a potential candidate for use as an anthelmintic agent. The study highlights the importance of targeting the tegument as a strategy for developing effective treatments against helminth infections.

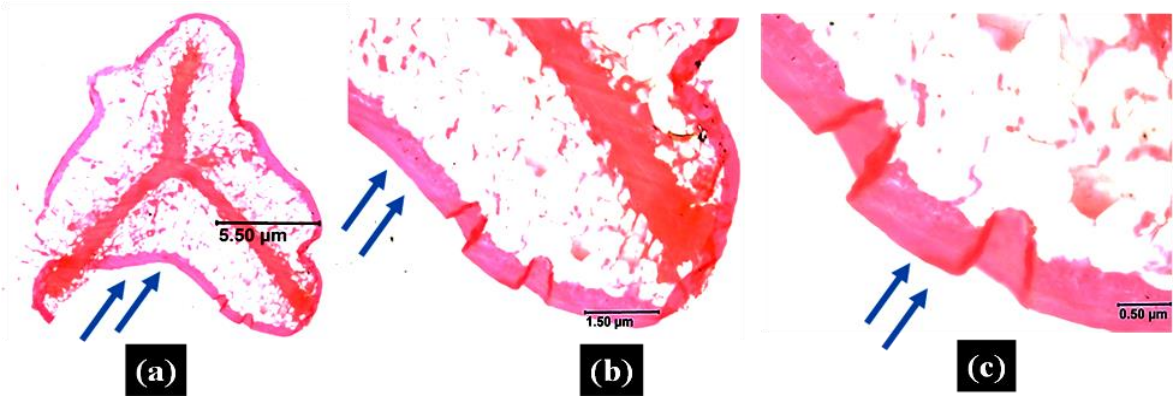

Figure 17. Histological sections of control parasite (a-c). Magnification, (a) 4x, (b) 20x, and (c) 40x, scale bar in µm

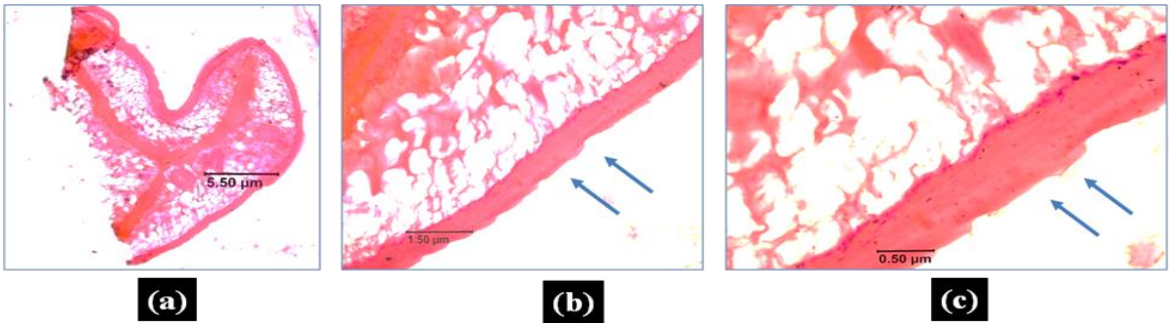

Figure 18. Histological sections of control parasite when treated with albendazole (a-c). Magnification, (a) 4x, (b) 20x, and (c) 40x, scale bar in µm

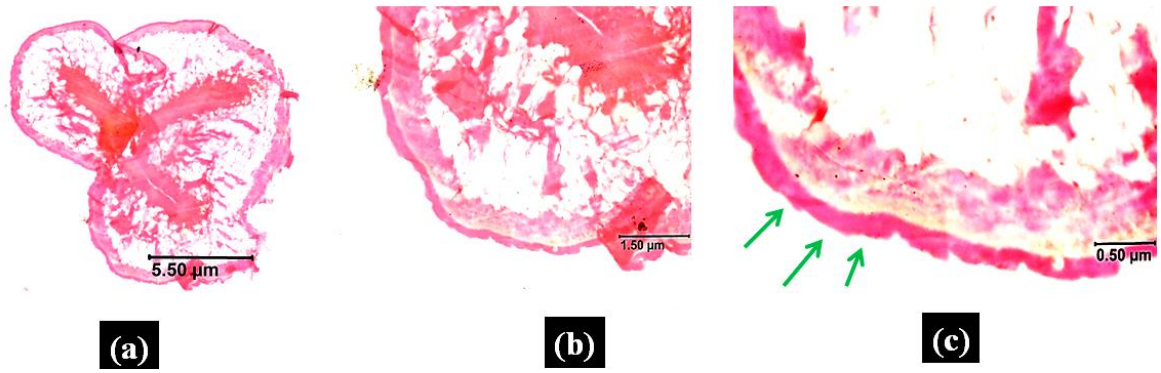

Figure 19. Histological sections of control parasite when treated with Diethyl ether extract (a-c). Magnification, (a) 4x, (b) 20x, and (c) 40x, scale bar in µm

4.8. Biochemical enzyme assay

Tegumental and glycolytic enzymes, such as phosphatases (e.g., acid and alkaline phosphatases), dehydrogenases (e.g., lactate and malate dehydrogenases), and neurotransmitter enzymes (e.g., acetylcholinesterase), play vital roles in the survival and metabolic processes of helminth parasites. These enzymes are involved in nutrient acquisition, energy production, immune evasion, and maintaining structural and functional integrity within the host. Targeting these enzymes provides a promising avenue for the development of novel anthelmintic drugs. Inhibiting these critical enzymes can disrupt the parasite's metabolism, compromise its ability to detoxify host-induced oxidative stress, and impair its neural signaling, ultimately leading to its death. This approach holds the potential for broad-spectrum efficacy, as many of these enzymes are conserved across various helminth species. Further research into selective enzyme inhibitors and their mechanisms of action could contribute to innovative therapeutic strategies for the effective management of helminth infections.

In the present study, the impact of DE extract on paralyzed helminth parasites was evaluated in comparison to control (untreated) and albendazole-treated parasites by assessing alterations in the activity of five critical enzymes essential for parasite survival. These enzymes included two glycolytic enzymes (malate dehydrogenase and lactate dehydrogenase), involved in energy metabolism; two tegumental enzymes (acid phosphatase and alkaline phosphatase), which play roles in nutrient uptake, immune modulation, and maintaining tegument integrity; and the neurotransmitter enzyme (acetylcholinesterase), crucial for neural signaling and motor function. Enzyme activity levels were quantified and compared across all groups, with albendazole-treated parasites serving as a reference standard. The findings indicate that treatment with DE extract induces significant alterations in enzyme activities, suggesting its potential to disrupt key metabolic and structural pathways in helminths, thereby supporting its development as a promising anthelmintic agent. Figure 20 presents the enzyme activity data for paralyzed helminth parasites treated with DE extract, albendazole, and compared to control (untreated) parasites. The activity of ACP was significantly reduced in DE-treated parasites, showing a concentration of 72.84 ± 2.37 µM/min/mg protein, compared to the control, which exhibited a concentration of 86.94 ± 3.17 µM/min/mg protein. Albendazole-treated parasites displayed a concentration of 74.26 ± 2.69 µM/min/mg protein. These results indicate a 16.21% reduction in ACP activity for DE-treated parasites and a 14.57%

reduction for albendazole-treated parasites, relative to the control. Similarly, the activity of ALP was also reduced in both treated groups. The control group showed a concentration of 880.33 ± 50.19 µM/min/mg protein, while DE-treated and albendazole-treated parasites exhibited concentrations of 505.33 ± 52.39 µM/min/mg protein and 492.77 ± 31.46 µM/min/mg protein, respectively. This indicates a 42.59% reduction in DE-treated parasites and a 44.02% reduction in albendazole-treated parasites compared to the control. These findings suggest that both DE extract and albendazole effectively reduce the activity of key tegumental enzymes, highlighting their potential to disrupt helminth parasite metabolism and structural integrity.

For MDH, the control parasites exhibited a concentration of 353.39 ± 38.87 nM/min/mg tissue protein, which was significantly higher compared to the DE-treated parasites, which showed a concentration of 274.03 ± 44.03 nM/min/mg tissue protein, reflecting a 22.45% reduction. Albendazole-treated parasites exhibited an even greater reduction, with a concentration of 224.42 ± 43.67 nM/min/mg tissue protein, showing a 36.49% reduction in activity. This indicates that while both DE extract and albendazole reduce MDH activity, albendazole treatment causes a more substantial decrease than DE extract. In the case of LDH, control parasites had a concentration of 213.41 ± 25.41 nM/min/mg tissue protein, which was markedly higher than the DE-treated parasites, which exhibited 147.26 ± 24.01 nM/min/mg tissue protein, reflecting a 39.75% reduction in activity. Albendazole-treated parasites showed a concentration of 134.92 ± 25.27 nM/min/mg tissue protein, which corresponds to a slightly smaller reduction of 36.90%. Both treatments caused a notable decrease in LDH activity, with DE extract showing a greater inhibitory effect compared to albendazole.

For AchE, the control parasites exhibited 30.43 ± 8.07 nM/min/mg protein, while DE-treated parasites showed a concentration of 19.57 ± 2.73 nM/min/mg protein, representing a 35.67% reduction in activity. Albendazole-treated parasites showed 20.86 ± 5.11 nM/min/mg protein, reflecting a 31.42% reduction. DE extract exhibited a stronger inhibitory effect on AchE compared to albendazole, suggesting that DE may be more effective in reducing acetylcholinesterase activity, which is critical for neural signaling and parasite movement. When comparing all the enzymes ALP demonstrated a more substantial reduction in activity whereas the inhibition of ACP was less pronounced, with showing a smaller reduction, suggesting that ACP may be less sensitive to DE extract. All five enzymes showed reduced activity in both DE extract and albendazole-treated parasites, with DE showing stronger inhibition for ALP, LDH, and AchE compared to albendazole.

However, ACP and MDH were less inhibited by DE extract than by albendazole. These results indicate that while both DE extract and albendazole are effective in reducing enzyme activities essential for helminth survival, DE extract may offer a more potent therapeutic effect for certain enzymes, particularly ALP, LDH, and AchE, which are critical for the parasite's metabolic and structural functions.

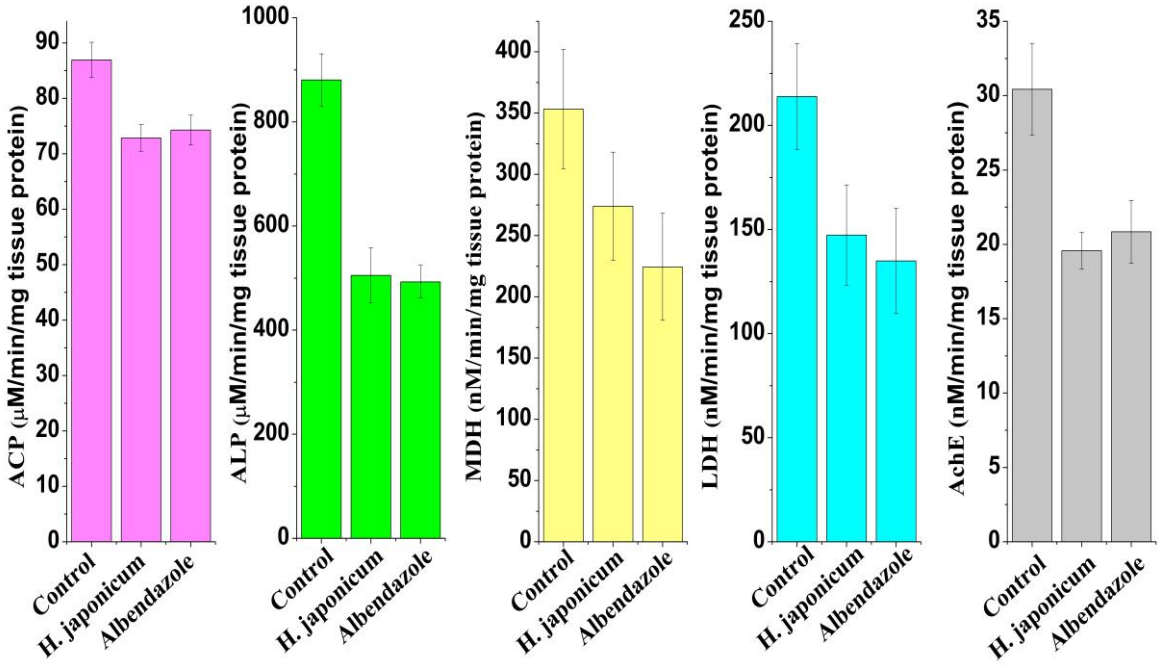

Figure 20. Acid phosphatase, Alkaline phosphatase, Malate dehydrogenase, Lactate dehydrogenase and Acetylcholinesterase enzyme, activity of control and plant extract treated parasite. Values are expressed as mean ± SD, n = 3 (three replicates). All the enzyme activities showed significant difference between control and plant extract-treated parasites at $P \leq 0.05$ level, except AchE enzyme

OBJECTIVE 2: Isolation, purification, and characterization of bioactive compound(s) from *Hypericum japonicum* and its anthelmintic study

4.9. Thin Layer Chromatography

Thin-layer chromatography (TLC) was employed to analyze the diethyl extract of *H. japonicum* in order to identify an effective solvent system for the separation of its components. Initially, small TLC slides (7.5x2.5 cm) were used to experiment with different solvent systems, specifically focusing on mixtures of petroleum ether and ethyl acetate in varying ratios. As illustrated in Photo plate 7, several ratios were tested to

determine which provided the best separation and resolution of the extract's components. After evaluating the results, a 1:1 ratio of petroleum ether and ethyl acetate (v/v) was chosen as the most suitable solvent system based on its ability to effectively separate the components of the extract. Following this, the selected solvent system (petroleum ether:ethyl acetate 1:1, v/v) was applied to a larger preparative TLC plate (21x17 cm), as shown in Photo plate 8. This allowed for a more extensive analysis and better separation of the active compounds present in the diethyl ether extract. Once the TLC run was completed, the plate was divided into four distinct sections—labeled A, B, C, and D—as shown in Photo plate 8. These sections were carefully collected and stored at -20°C for future use, ensuring that the separated compounds could be further analyzed or used for additional experiments. The successful identification of an appropriate solvent system and the isolation of specific fractions for further study will contribute to the understanding of the chemical composition and potential bioactive properties of *H. japonicum*.

I. Diethyl ether extract

The TLC run on a larger preparative slide (21x17 cm) for the diethyl extract of *Hypericum japonicum* led to the collection of distinct fractions, each containing varying amounts of separated compounds. Section **A** yielded approximately 15 g, section **B** yielded 12 g, section **C** yielded 2 g, and section **D** yielded 6 g. To prepare the diethyl extract, 50 g of powdered *H. japonicum* was soaked in diethyl ether, and the mixture underwent three rounds of filtration to remove plant material and other impurities. After the filtration process, approximately 0.3 to 0.5 g of concentrated extract was obtained, which was then stored at -20°C to preserve its stability for future use. These fractions were further analyzed to identify the chemical components present and evaluate their potential bioactive properties. This process is crucial for isolating and characterizing the active compounds of *H. japonicum*, which could have significant pharmacological applications. The stored extract will be used in subsequent experiments, such as cytotoxicity, antioxidant, or antimicrobial assays, to assess its therapeutic potential.

II. In-vitro anthelmintic study

The anthelmintic study was done in *Paramphistomum* spp. for the different sections of the extracts extracted from TLC. Two doses were taken 5 mg/mL and 10 mg/mL. Paralysis time and death time were recorded. Table 8 shows the anthelmintic activity. The strongest

anthelmintic activity was found to be the section “A” with death time of 69:11 ± 9:56 h:min at 5 mg/mL and 61:18 ± 16:44 h:min at 10 mg/mL followed by sections C, B, and D as shown in the table 8. The control parasites survived upto 131:21+1:36 (h:min). The repeation of the study was done for three times.

Table 4. Anthelmintic activity of different fractions of *Hypericum japonicum*

Sample	FR	Dose	Paralysis time (h:min)	Death Time (h:min)	Dose	Paralysis time (h:min)	Death Time (h:min)
Hypericum japonicum (DE TLC)	A	5 mg/ml	68:48 ± 9:57	69:11 ± 9:56	10 mg/ml	60:03 ± 16:21	61:18 ± 16:44
	B		85:16 ± 6:42	85:30 ± 6:43		81:01 ± 16:02	82:15 ± 17:12
	C		74:54 ± 13:15	75:7 ± 13:24		66:03 ± 07:49	66:54 ± 07:48
	D		88:50 ± 6:43	89:03 ± 6:45		87:06 ± 12:07	87:18 ± 11:06

Control parasite lived up to 131:21+1:36 (h:min). Values are expressed as mean ± SD, n = 3 (no. of experiments), FR - fractions

4.10. Column chromatography

I. Liquid Chromatography- Mass spectrometry (LC-MS) analysis

The LC-MS analysis, utilizing Electrospray Ionization (ESI), was conducted in the 0 to 450 m/z range to identify the compounds present in the section "A" TLC extract of *Hypericum japonicum*, which showed the best anthelmintic activity. In negative ESI, molecules acquire an extra electron, resulting in a negatively charged ion. This technique is particularly useful for analyzing molecules with higher electron affinity or those that are more acidic, such as carboxylic acids, phenolic compounds, fatty acids, and nucleotides. The analysis aimed to identify compounds with high relative abundance in the given m/z range. Among the compounds detected, the highest relative abundance was observed at an m/z value of 160.690, followed by 300.90. The chromatogram displaying various peaks is shown in Figure 21. Based on literature, **quercetin** was selected for further study as a potential bioactive compound from the TLC A fraction, identified by its m/z value of 300.90, which corresponds to the molecular weight of quercetin (302.23 g/mol). No compounds with an m/z value of 160.690 were found to have anthelmintic properties. To

confirm the presence of quercetin in the extract, High-Performance Liquid Chromatography (HPLC) was subsequently performed.

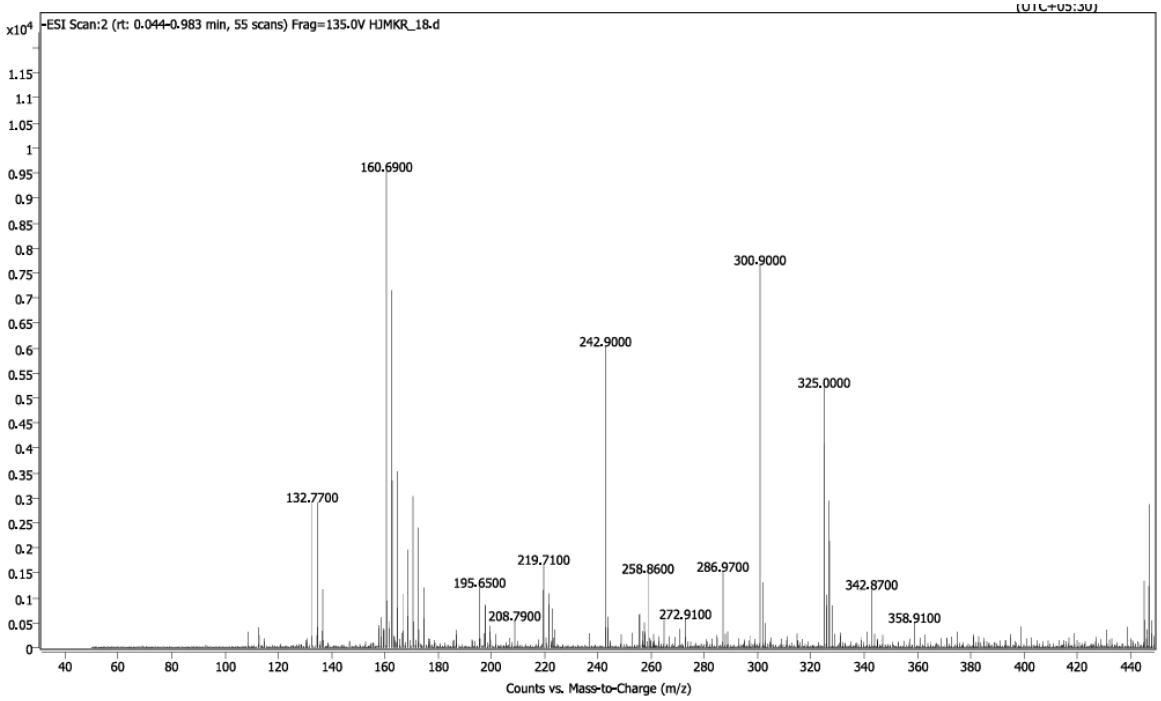

Figure 21. LC-MS chromatogram of TLC (fraction A) extract of *Hypericum japonicum* (diethyl ether extract)

II. High-performance liquid Chromatography (HPLC)

The HPLC profile has been shown in Figure 22. From the LC-MS study as our target compound was Quercetin so a standard was prepared with the Quercetin in HPLC. TLC fraction "A" extract was then inserted in the HPLC for the confirmation of the bioactive compound. From the profile, it can be concluded that Quercetin is present at peak 4.015. The quantity of Quercetin presence shown was 225.208 ppm. Therefore, by HPLC it is confirmed that Quercetin is present in the TLC fraction A. The IUPAC name of the compound thus identified is 2-(3,4-dihydroxyphenyl)-3,5,7-trihydroxychromen-4-one. The molecular formula of the compound is $C_{15}H_{10}O_7$. The molecular weight of the compound is 302.23 g/mol. It appears as yellow needles or yellow powder. It was then purchased from SIGMA-Aldrich for further study.

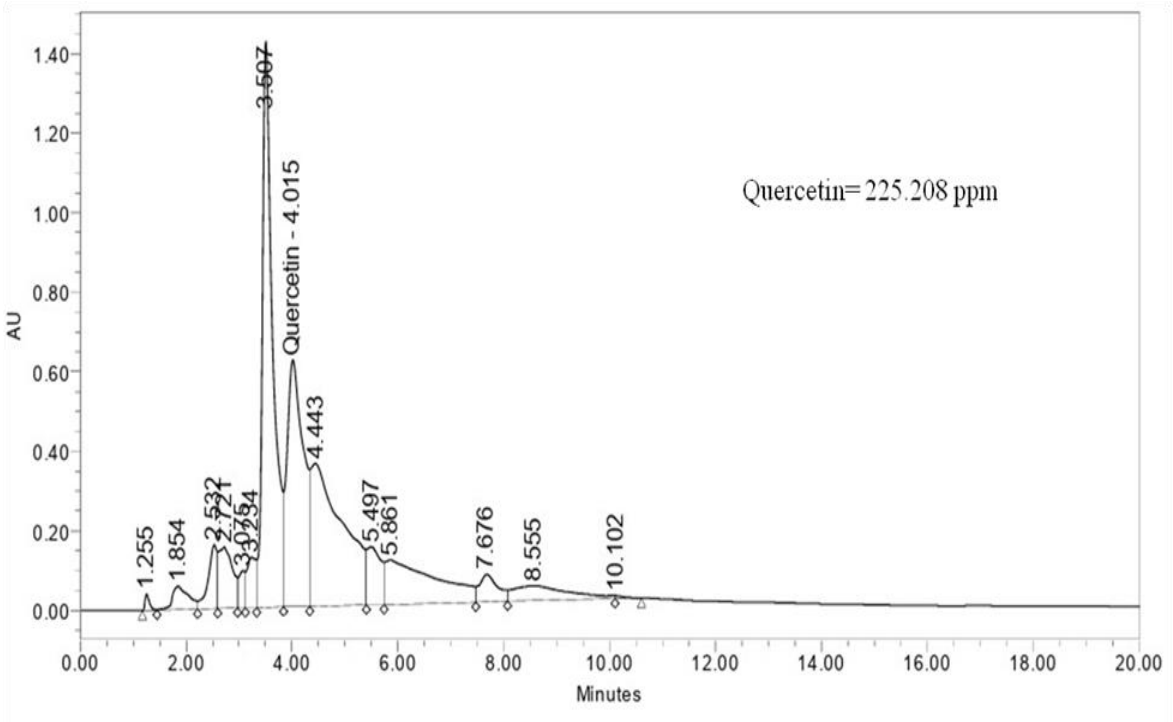

Figure 22. HPLC chromatogram of TLC (fraction A) extract of *H. japonicum* (diethyl ether extract)

4.11. In-vitro anthelmintic study with active compound (Quercetin)

The anthelmintic study was done in *Paramphistomum* spp. with the bioactive compound (Quercetin) indentified from the plant. Three doses were taken 0.5 mg/mL, 1 mg/mL and 10 mg/mL. Paralysis time and death time were recorded. It has shown good anthelmintic activity. The time taken for the death of the parasites in 0.5 mg/mL were 23:22 ± 3:12 h:min, again in 1 mg/mL the time taken for death of the parasites were 18:31 ± 6:31 h:min. Similarly, at 10 mg/mL also shown good acitivity with time taken for death of the parasites was 13:08 ± 8:24 h:min. The paralysis time as well as death time has been shown in the table 9. The time taken for the death of the parasite by the reference drug at 10 mg/mL were 17:19 ± 6:19 h:min. Here, the compound quercetin has shown better activity than the reference drug albendazole. The control parasites survived upto 143:21+1:33 (h:min). The repeation of the study was done for three times.

Table 5. Anthelmintic activity of quercetin with different doses

Compound	Dose	Paralysis time (h:min)	Death Time (h:min)
Quercetin	0.5 mg/ml	22:48 ± 4:11	23:22 ± 3:12
	1 mg/ml	17:41 ± 6:17	18:31 ± 6:21
	10 mg/ml	12:25 ± 8:37	13:08 ± 8:24
Albendazole	10 mg/ml	17:02 ± 6:15	17:19 ± 6:19

Values are expressed as mean ± SD, n = 3 (no. of experiments)

OBJECTIVE 3. Study of histological, ultrastructural, and biochemical alterations in helminth parasites treated with bioactive compound(s)

4.12. Histological study with quercetin

A histology study was of control, quercetin treated and albendazole treated parasite was done. The visualization was taken on 4X, 20X, and 40X. Like our earliar study, mainly the tegument section were studied and focused. Figure 23 shows the images of the control parasite. It is visible that the tegument of the control parasite is fine and smooth without any ruptures. Figure 24 shows the tegument of the parasite treated with quercetin which shows clear breakage and roughness of the outer layer of the tegument and figure 25 shows the histological images of parasite treated with the reference drug (albendazole). It also shows that the tegument has become rough and continous breakage has been observed in the cuticle of the helminth parasite.

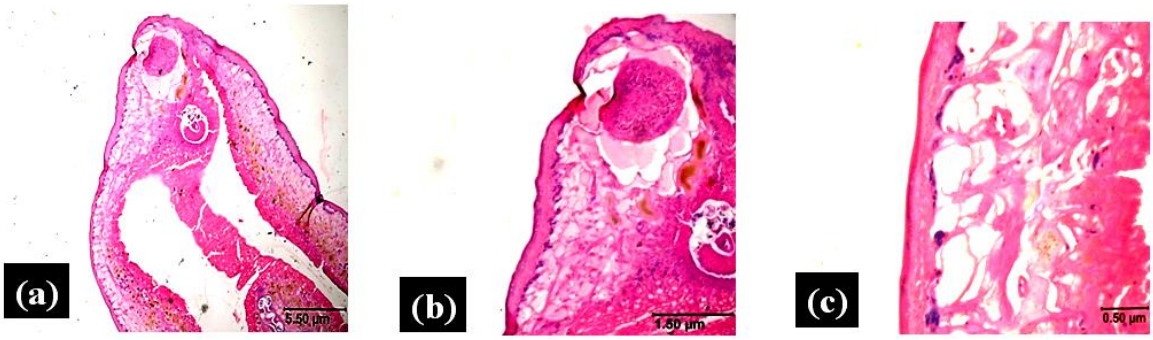

Figure 23. Histological sections of control parasite (a-c). Magnification, a= 4x, b=20x, and c=40x, scale bar in micrometer (µm)

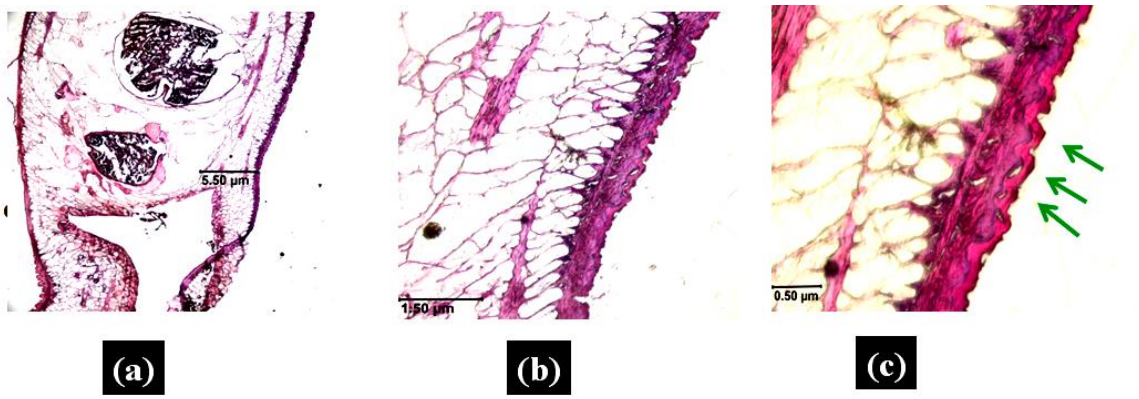

Figure 24. Histological sections of parasite treated with quercetin (a-c). Magnification, a=4x, b=20x, and c=40x, scale bar in micrometer (µm)

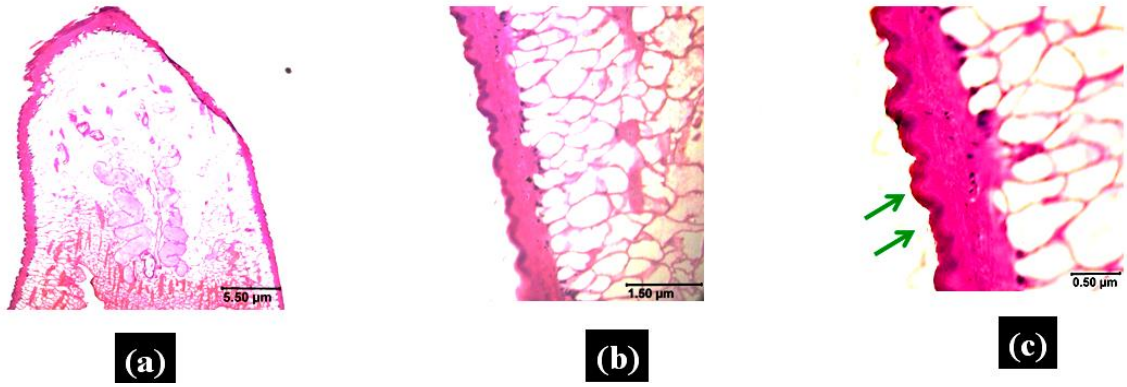

Figure 25. Histological sections of parasite with albendazole (a-c). Magnification, a= 4x, b= 20x, and c=40x, scale bar in micrometer (µm)

4.13. Scanning Electron Microscopy

SEM study was done to see condition of the body surface and tegument of the paralyzed parasites after the treatment with the compound quercetin and the reference drug albendazole. The SEM study of the untreated parasites also done for the comparison. Figure 26 shows scanning electron microscopy of control helminth parasite. The parasite exhibited smooth boy surface. The tegument of the control parasite also remained smooth. The body also didn't get much shrinkage. Whereas, when observed the SEM of the treated parasites with quercetin, it was clearly visible that the body got shrinkage compared to the control parasite. The surface of the body of the parasite turned rough and seen breakage

through out the body. Distortion of the cuticle is seen with breakage of the tegument of the parasite as shown in figure 27. Simialarly, the parasite treated with albendazole also shown breakage, roughness, shrinkage of the body surface and cutile breakdown through out the body as shown in figure 28.

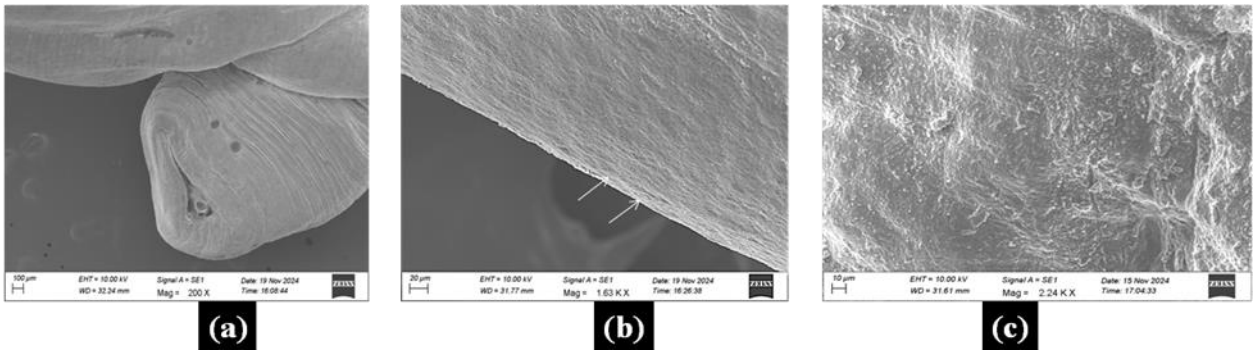

Figure 26. Scanning electron micrographs of control parasite (a & b) showing the tegument part with scale 100 µm and 20 µm, and (c) Body surface of control parasite with scale 10 µm

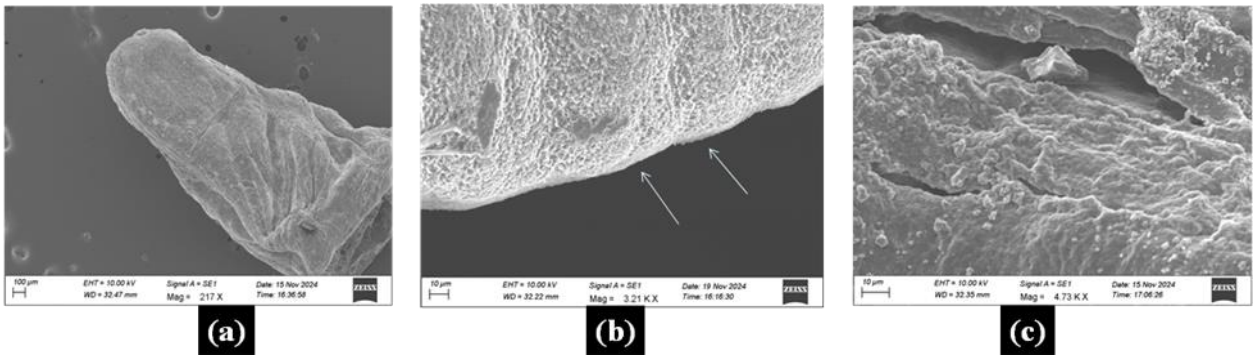

Figure 27. Scanning electron micrographs of quercetin treated parasite (a & b) showing the tegument part with scale 100 µm and 10 µm, and (c) Body surface of control parasite with scale 10 µm

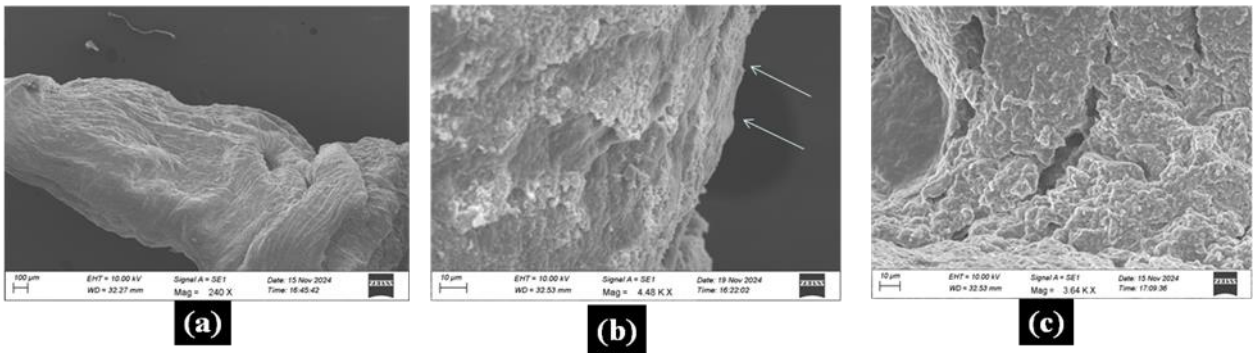

Figure 28. Scanning electron micrographs of albendazole treated parasite (a & b) showing the tegument part with scale 100 µm and 20 µm, and (c) Body surface of control parasite with scale 10 µm

4.14. Biochemical Enzyme Assay

For biochemical enzyme study, the paralyzed parasite treated with quercetin was taken along with the control and Alb treated parasites. Like our earlier study, five enzymes malate dehydrogenase, lactate dehydrogenase, acid phosphatise, alkaline phosphatise acetylcholinesterase were taken. It has been investigated to see whether there is any alteration in the enzyme activities in untreated, quercetin treated and Alb treated helminth parasites. The activities of the enzymes were shown in Figure 29. Paralyzed parasites treated with quercetin and Alb showed a decrease in ACP with control parasites showing concentration of 87.95 ± 0.97 µM/min/mg protein whereas quercetin treated parasites has shown concentration of 61.10 ± 2.26 µM/min/mg protein and the Alb treated has shown concentration of 66.75 ± 1.54 µM/min/mg protein. Thus, quercetin treated has shown a reduction of 26.85 % and Alb treated has shown a reduction of 21.20 % from the control parasites. ALP has also shown decrease in activity when compared with untreated parasites. The control has shown concentration of 859.85 ± 15.12 µM/min/mg protein, while the concentration of quercetin treated and Alb treated parasites has shown concentrations of 439.71 ± 14.86 µM/min/mg protein and 449.59 ± 6.90 µM/min/mg protein, respectively. Clearly, there is a reduction in concentration with 48.86 % in quercetin treated and 47.71 % in Alb treated parasites.

For the MDH, the control parasites has shown concentration of 307.09 ± 14.91 nM/min/mg tissue protein, while quercetin treated parasites has shown activity of 201.05 ± 418.12 nM/min/mg tissue protein and Alb treated has shown activity of 267.03 ± 19.48 nM/min/mg tissue protein. Here, the quercetin treated has shown reduced in activity by 34.52 % and Alb treated by 12.77%. LDH has also shown decrease in activity from control parasites with control parasites showing 211.64 ± 34.36, nM/min/mg tissue protein, and quercetin treated showing 140.21 ± 23.65, nM/min/mg tissue protein and Alb treated showing 127.86 ± 33.75, nM/min/mg tissue protein. Thus, quercetin treated showing reduced in activity by 38.24 % and Alb treated by 39.58 %. In AchE, the control has shown concentration of 29.57 ± 3.10 nM/min/mg protein, whereas quercetin treated parasites has shown concentration of 19.57 ± 2.54 nM/min/mg protein and Alb treated parasites has shown concentration of 17.79 ± 2.67 nM/min/mg protein. Here, the quercetin treated has shown decrease in activity by 33.83 % and Alb treated by 39.84 %. Therefore, all the five enzymes showed reduced activity in quercetin and Alb treated parasites. The enzyme activities showed significant differences at $P \leq 0.05$ with the control, except AchE. The

highest percentage of inhibition of quercetin was found in ALP and the least was found in ACP.

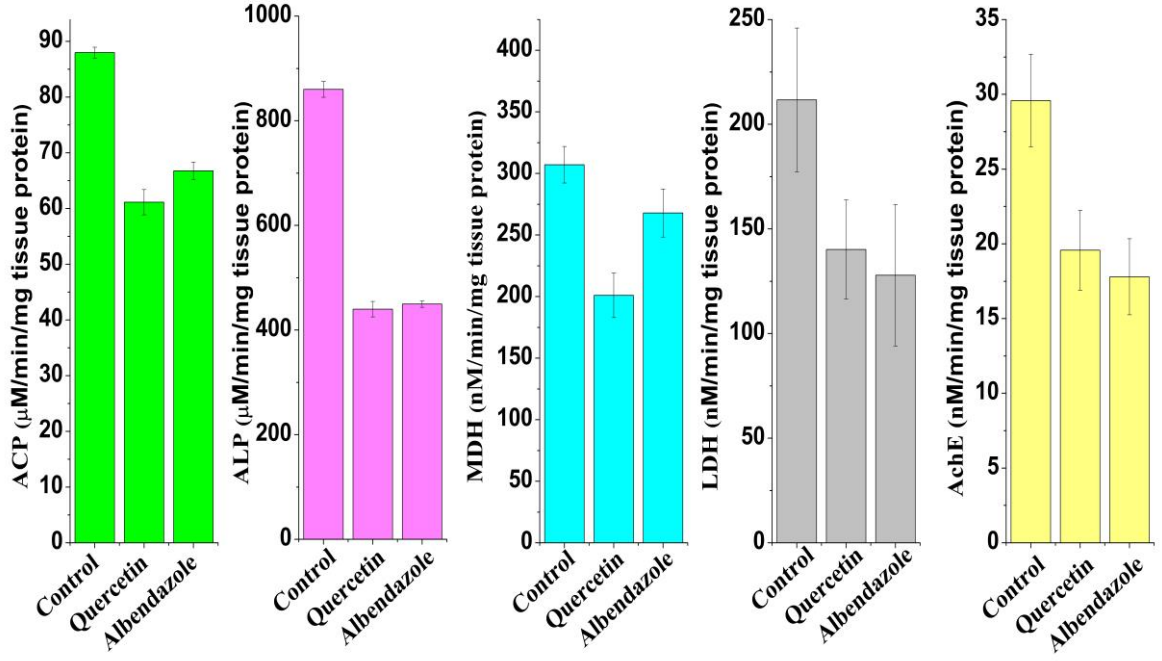

Figure 29. Acid phosphatase (ACP), Alkaline phosphatase (ALP), Malate dehydrogenase (MDH), Lactate dehydrogenase (LDH), and Acetylcholinesterase (AchE) enzyme, activity of control, quercetin and albendazole treated parasite. All the enzyme activities showed significant difference between control and treated parasites at $P \leq 0.05$ level, except AchE enzyme

OBJECTIVE 4: Evaluation of molecular interaction and docking of bioactive compound(s) with enzymes using bioinformatics tools

4.15. Protein modeling and Molecular docking with the best solvent extract

Protein modeling was carried out using the Swiss-Model server. The templates used were 2hpa.1.A, 3mk1.1.A, 4l4s.1.A, 2dfd.1.A, and 5fpq.2.A for ACP, ALP, LDH, MDH, and AchE enzymes, respectively. The model protein and the template of AchE has been shown in the Figure 30. The model protein and the template of ACP has been shown in the Figure 31. The model protein and the template of ALP has been shown in the Figure 32. The

model protein and the template of LDH has been shown in the Figure 33. And the model protein and the template of MDH has been shown in the Figure 34.

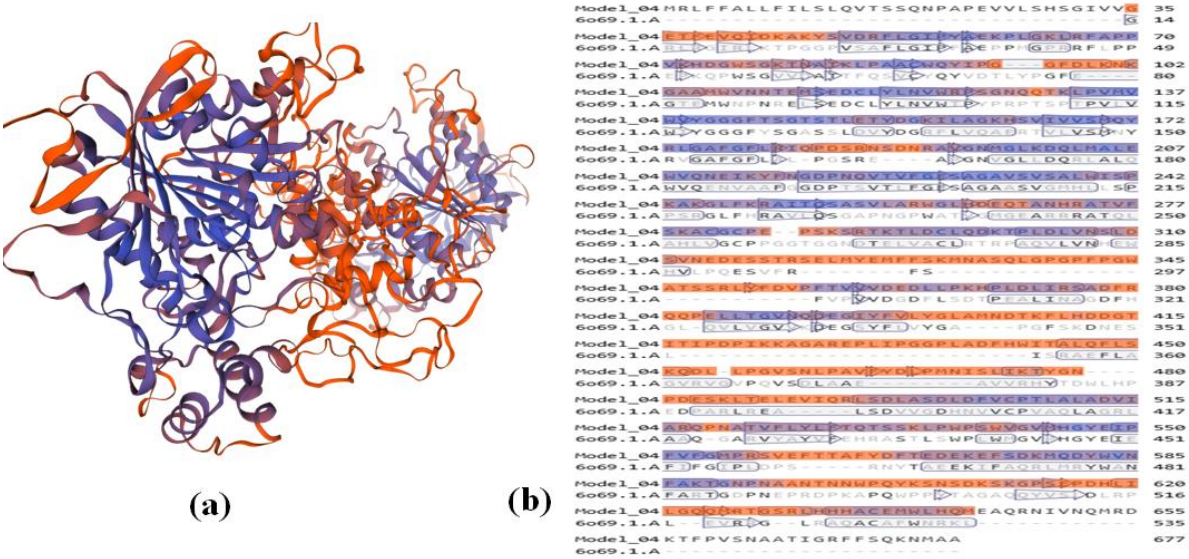

Figure 30. Structural assessment of Acetylcholinesterase; (a) model, and (b) template protein

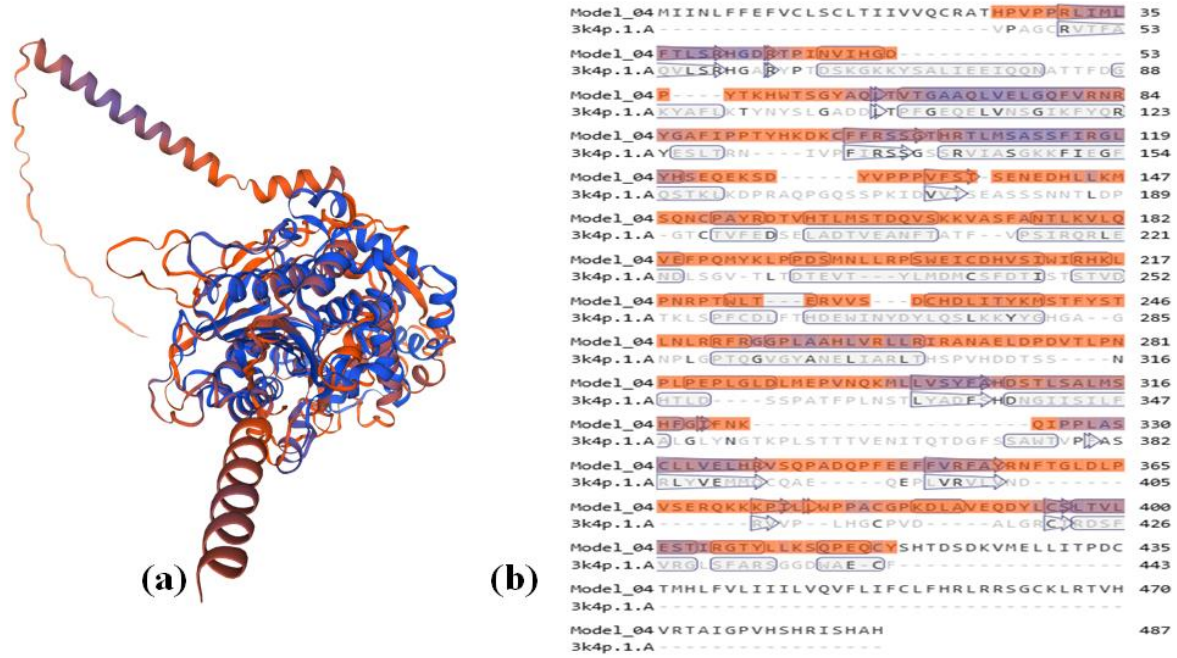

Figure 31. Structural assessment of Acid phosphatase; (a) model, and (b) template protein

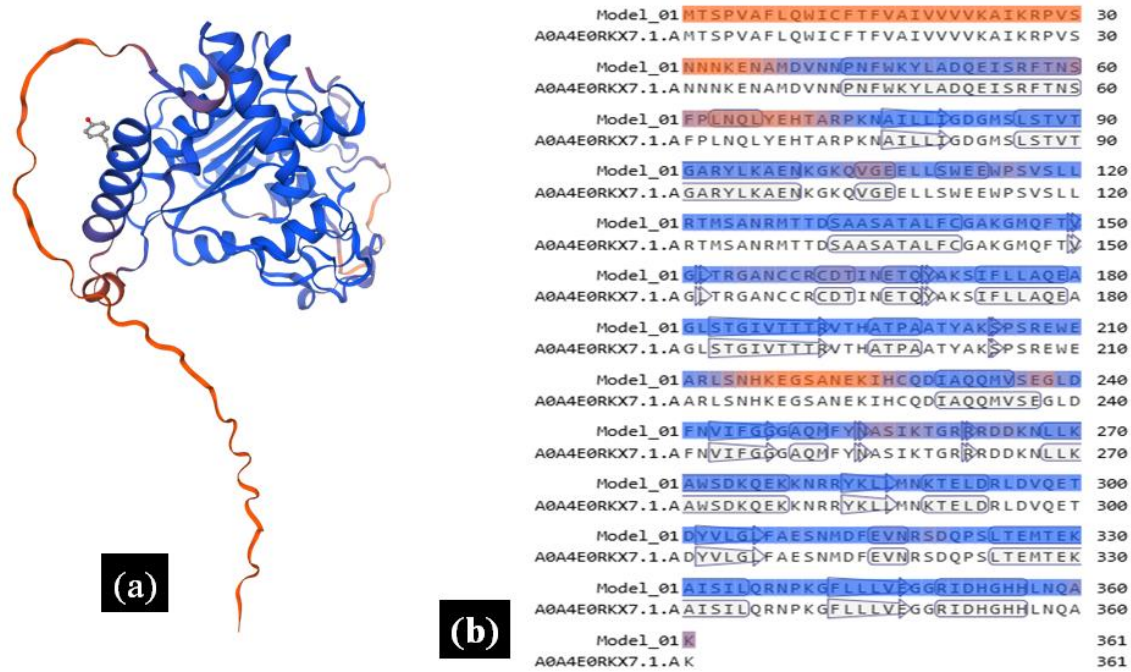

Figure 32. Structural assessment of Alkaline phosphatase; (a) model, and (b) template protein

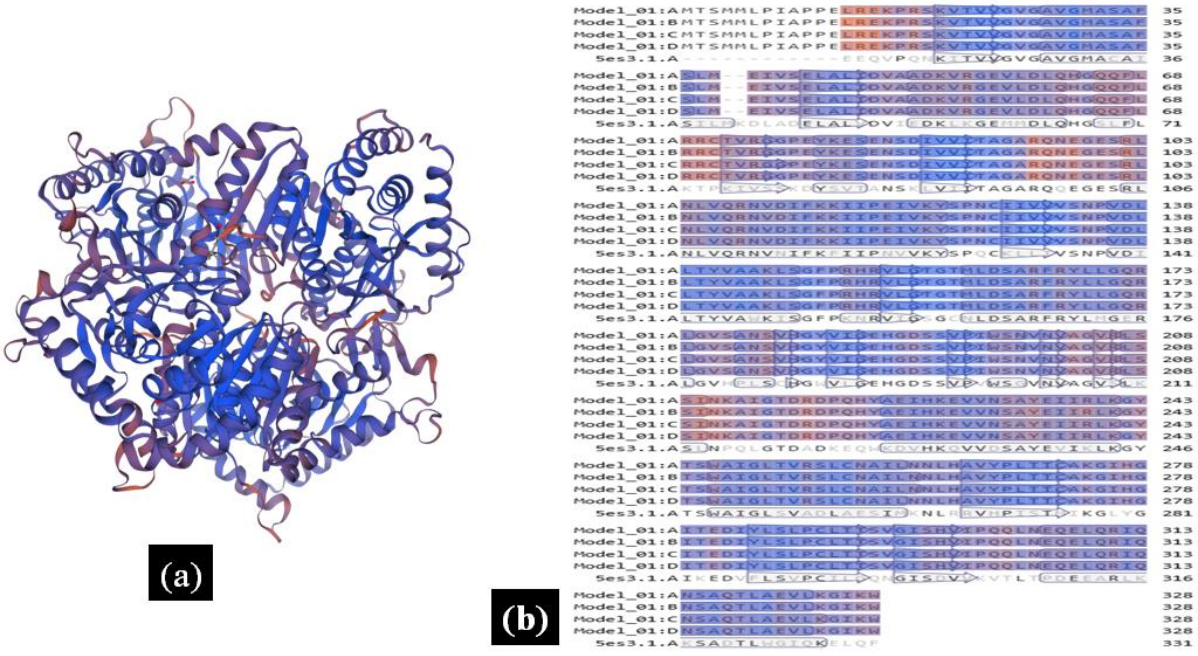

Figure 33. Structural assessment of Lactate dehydrogenase; (a) model, and (b) template protein

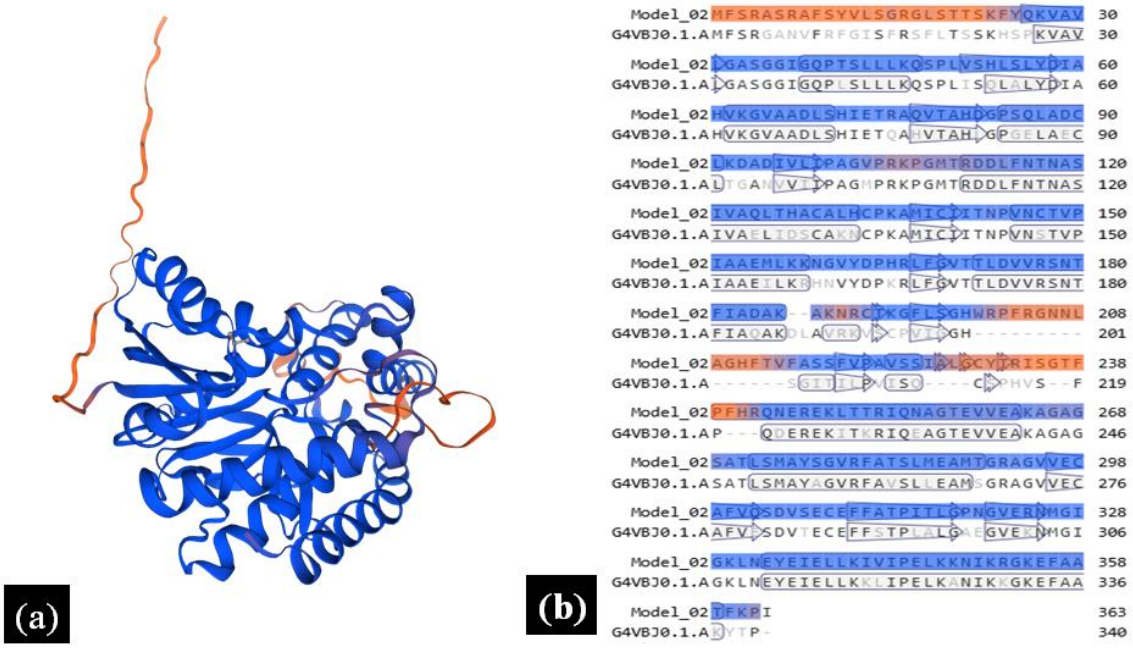

Figure 34. Structural assessment of Malate dehydrogenase; (a) model, and (b) template protein

4.16. Docking study

Molecular docking studies were performed to evaluate the binding affinity of Quercetin with five model enzymes. The 2D and 3D structures of Quercetin are shown in Figure 35, while Table 10 presents the binding affinities of the compound with each enzyme. The docking results revealed that Quercetin exhibited the strongest interaction with Acetylcholinesterase (AchE) (-7.8 kcal/mol) and Alkaline Phosphatase (ALP) (-7.6 kcal/mol), indicating its potential as a bioactive compound against these targets. In contrast, the weakest binding affinity was observed with Acid Phosphatase (ACP) (-3.5 kcal/mol). These findings suggest that Quercetin may have a stronger inhibitory potential for AchE and ALP, which are associated with neurological and metabolic processes, respectively.

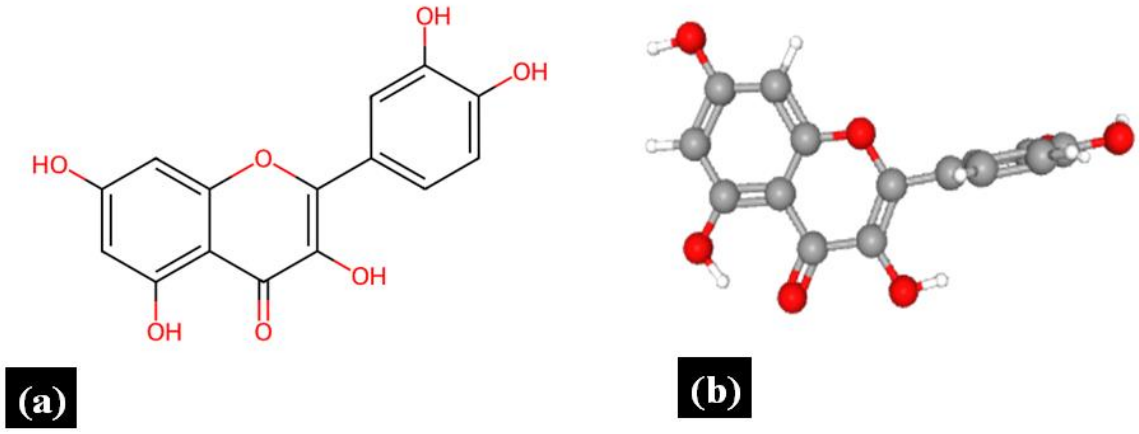

Figure 35. Structure of quercetin, a) 2D and b) 3D

Table 6. Binding energies (-kcal/mol) of *Hypericum japonicum* phytocompounds with different enzymes

Compounds	AchE	ACP	ALP	LDH	MDH
Quercetin	-7.8 ± 0	-3.5 ± 0.17	-7.6 ± 0	-6.7 ± 0	-6.8 ± 0
Albendazole	-6.6 ± 0	-2.7 ± 0.43	-6.5 ± 0	-5.56 ± 0.15	-5.46 ± 0.15

All dockings are carried out for triplicate. Values are expressed as mean ± SD, n=3 (no. of dockings).

The reference drug Albendazole, commonly used as an anthelmintic agent, was also subjected to docking analysis for comparative evaluation. Similar to Quercetin, Albendazole exhibited the highest binding affinity with AchE (-6.6 kcal/mol) and the lowest with ACP (-2.7 kcal/mol). While both compounds followed the same trend in binding affinities across the enzymes, Quercetin consistently demonstrated stronger interactions, particularly with AchE and ALP. This suggests that Quercetin might have superior bioactivity compared to Albendazole in targeting these specific enzymes.

Figure 36 displays the 2D binding interactions of quercetin with various proteins, while Figure 37 provides a 3D superimposition of the binding interactions between the proteins and quercetin, compared to the reference drug albendazole. The 3D superimposition shows that the positions of interaction for quercetin and albendazole are strikingly similar, suggesting that both compounds interact with the same or similar binding sites on the protein structures. Quercetin exhibited strong binding affinity with AchE, with a total of 14 residues involved in the interaction, including 2 conventional hydrogen bonds with Arg A:299 and Leu A:287, 2 non-classical hydrogen bonds with Arg

A:299 and Arg A:174, 1 Pi-carbon bond with Arg A:299, 3 mixed pi-alkyl interactions with Leu A:287, Arg A:299, and Arg A:174, 1 Pi-sigma bond with Thr A:288, 2 unfavorable bonds with Pro A:170 and Ser A:300, and 3 van der Waals interactions. Additionally, quercetin interacts with other proteins, including ALP, with 17 residues showing 3 conventional hydrogen bonds, 1 carbon H-bond, 2 pi-alkyl interactions, 1 pi-anion interaction, 1 unfavorable bond, and 9 van der Waals interactions; ACP, with 7 residues showing 1 conventional hydrogen bond, 2 pi-alkyl interactions, 1 pi-sigma bond, 1 unfavorable bond, and 2 van der Waals interactions; LDH, with 16 residues showing 4 conventional hydrogen bonds, 1 carbon H-bond, 1 pi-alkyl interaction, 2 pi-sigma interactions, and 7 van der Waals interactions; and MDH, with 8 residues showing 3 conventional hydrogen bonds, 1 non-classical hydrogen bond, 1 pi-cation interaction, 1 pi-hydrophobic interaction, and 4 van der Waals interactions. These results demonstrate that quercetin forms a diverse array of interactions with several proteins, including hydrogen bonds, pi-based interactions, and van der Waals forces. The similarity in binding positions between quercetin and albendazole suggests that quercetin may share similar mechanisms of action, particularly with AchE, where it shows the best binding affinity, highlighting its potential as a promising ligand for various protein targets and suggesting its therapeutic value.

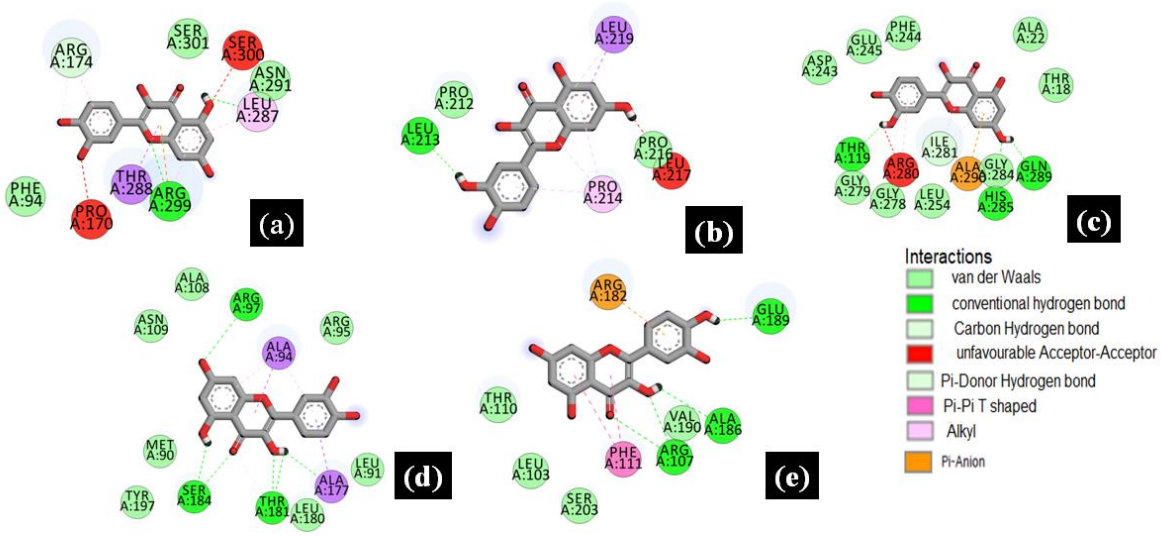

Figure 36. 2D binding affinities of enzymes and Quercetin (Q) (a) AchE & Q (b) ACP & Q, (c) ALP & Q (d) LDH & Q , and (d) MDH & Q

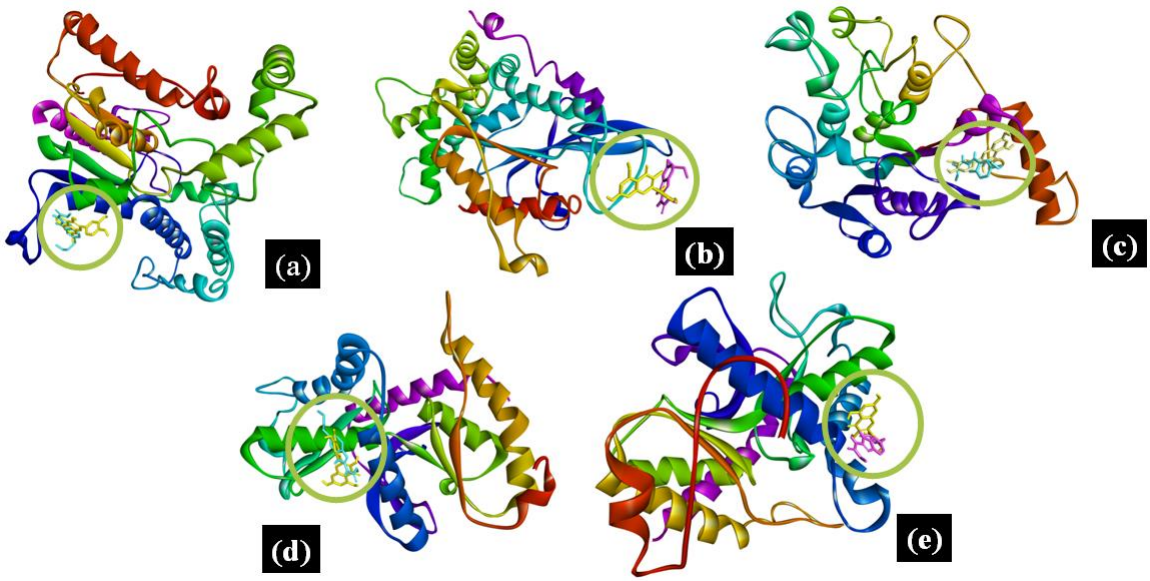

Figure 37. Molecular docking and 3D binding affinities of enzymes and Quercetin (a) AchE & Q (b) ACP & Q, (c) ALP & Q (d) LDH & Q and (e) MDH & Q. Ligand colour: quercetin = yellow, albendazole = purple and cyan

4.17. Analysis of drug-likeness and ADMET profile

The bioactive compound (Quercetin) and the reference drug (Albendazole) were evaluated for their drug-likeness properties using the online databases. The drug-likeness properties of both the compounds as evaluated according to the Lipinnski's rule of five (Ro5) are summarized in table 10. According to Lipinnski's rule of five, it tells that a drug is orally active if the molecular weight of the drug is less than 500g/mol, LogP≤5, Hydrogen Bond Donor (HBD≤5), Hydrogen Bond Acceptor (HBA≤10) and the topological polar surface (TPSA≤ 140 Å²). The rule also says that an orally active drug should not violate more than one criteria. Quercetin and Albendazole showed strong drug-likeness property as it followed all the Ro5. Thus, quercetin can be considered as a good oral drug.

Table 7. Lipinski's data of drug-likeness properties

Compound	PubChem ID	Molecular formula	Molecular weight	LogP (≤5)	HBD (≤5)	HBA (≤10)	TPS (A²)
Quercetin	5280343	$C_{15}H_{10}O_7$	320.23	1.54	5	7	131.36
Albendazole	2082	$C_{12}H_{15}N_3O_2S$	265.33	2.81	2	3	92.31

In addition to evaluating drug-likeness properties, this study further investigated the potential pharmacokinetic properties of the quercetin and albendazole using various bioinformatic tools. Figure 38 shows the ADMET properties of the quercetin and the albendazole. Quercetin has shown moderate absorption by the human intestine whereas albendazole has shown low human instestinal absoption. For F (20% Bioavailability), both the compounds has shown good absoption as they have shown almost similar absoption more than 0.5 and for F (30% Bioavailability) also it has querectin has better result with 0.493 and albendazole with 0.329. Thus, because of having a good absortion property the compound will able to penetrate and reach to the cell membrane and also reach its target site. The quercetin has shown less permeability to blood-brain barrier (BBB) with only probability of 0.264 which can also be considered as good drug-likeness property. Whereas, albendazole has shown very high permeability to BBB with probability of 0.962. Cytochrome P450 (CYP) enzyme is a group of enzyme superfamily that play a crucial role in the metabolism and detoxification of drugs. Quercetin has shown less P450 inhibitory and substrate metabolism properties except for Cytochrome P450 CYP1A2 inhibitor and P450 CYP3A4 inhibitor where it has shown high inhibitory property. Whereas, albendazole has shown better Cytochrome P450 (CYP) inhibitory and substrate metabolism compared to quercetin. The half life property shown by the quercetin is low, it shows half life property ($T_{1/2}$) of 0.2 h (which is less than <3). It has also predicted having slow clearance rate of 2.045 mL/min/kg (<5 mL/min/kg) which indicates good bioavailability. Albendazole has also shown lower half life property and clearance rate than quercetin with 1.24 h (($T_{1/2}$) and 1.471 mL/min/kg clearance rate. Quercetin has also shown very minimal toxilogical properties except for AMES which has shown moderate and for DILI it has shown high probability, whereas albendazole has hown high toxicity property for H-HT, DILI and FADMMD. Thus, the present study shows that, the bioactive compound quercetin has shown good ADMET properties in most of the parameters, suggesting their good drug-likeness property.

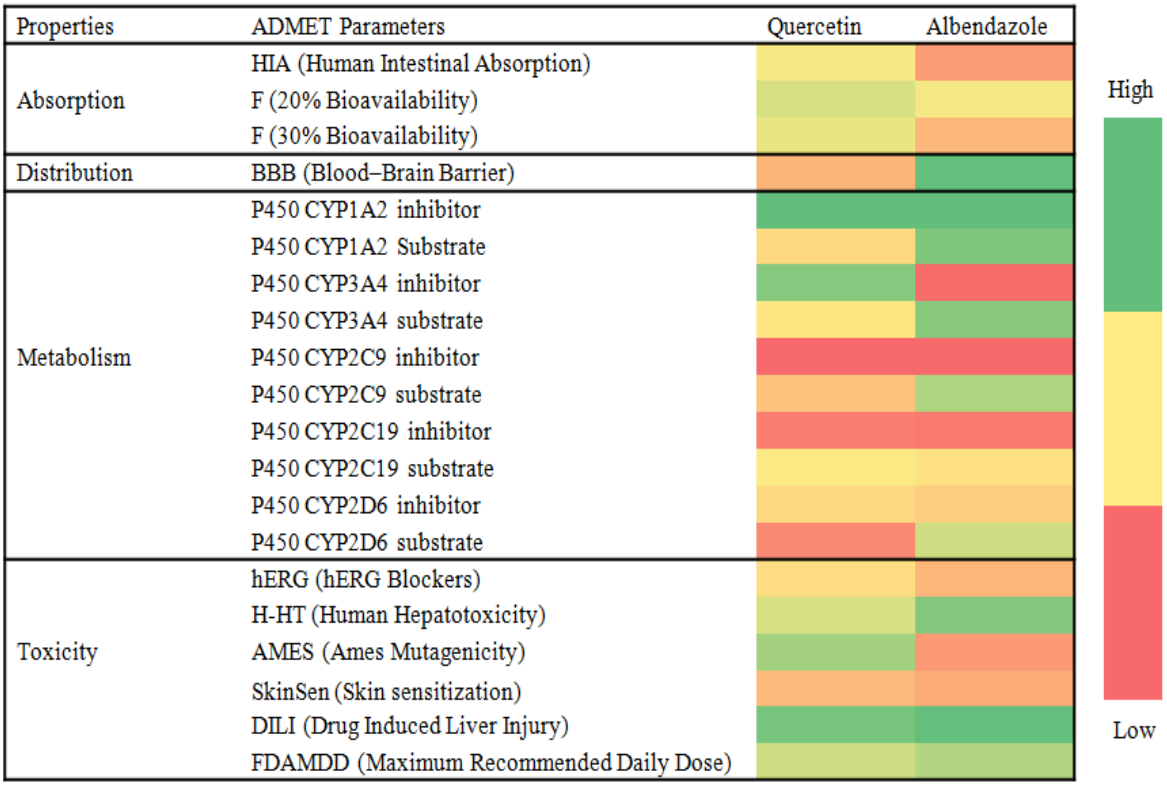

Figure 38. ADMET properties of quercetin and albendazole

4.18. Molecular Dynamics Simulation Study

Molecular Dynamics (MD) simulation is a powerful computational tool widely used in biological sciences to study the structural dynamics and interactions of biomolecules at an atomic level. It provides critical insights into protein-ligand interactions, conformational changes, and binding stability over time, which are essential for understanding molecular mechanisms in drug discovery, enzyme function, and biomolecular interactions. Figure 39 displays a 2D representation, and Figure 40 provides a 3D visualization of the binding affinities of the protein-ligand complex at five distinct time intervals during the MD simulation. These Figures collectively illustrate how the protein-ligand interactions evolve over time, highlighting important changes in binding patterns and affinities. At 10 ns, the protein-ligand complex showed interactions involving a total of 11 residues. Of these, 1 conventional hydrogen bond (H-bond) was observed, which indicates a specific polar interaction between the ligand and the protein's functional groups. Additionally, 6 van der Waals interactions were noted, reflecting the non-polar interactions that stabilize the complex by promoting close-range contact between the ligand and the protein's hydrophobic surfaces. At 20 ns, a shift in the binding interactions was observed, with only

8 residues involved. This reduction suggests that some initial interactions may have weakened or altered due to changes in the ligand or protein structure. During this interval, there was still 1 H-bond, but an increase in the number of van der Waals interactions (7) was observed. This shift could indicate that the ligand's conformation adapted to favor non-polar interactions as the complex continued to stabilize.

By 50 ns, the binding interactions began to stabilize further, with 9 residues engaged in binding. At this stage, there was an increase in H-bonds to 2, indicating that the ligand's positioning within the protein binding site had evolved to form more stable and specific interactions. Additionally, 2 van der Waals interactions were observed, suggesting that while non-polar interactions were still important, the complex now exhibited a more balanced mix of both polar and non-polar stabilizing forces. At 70 ns, the number of residues involved in the binding interactions remained at 9, but there was a reduction in the number of van der Waals interactions (3) compared to the previous time points. Despite this decrease, the ligand still maintained 1 H-bond, which suggests that the protein-ligand complex may have reached a more dynamic or flexible binding state. Finally, at 100 ns, the binding interaction remained relatively stable, involving 9 residues, with 1 H-bond and 4 van der Waals interactions. The increase in van der Waals interactions at this point could indicate a stabilization of the ligand's position in the binding pocket, where it now interacts more extensively with the hydrophobic regions of the protein. The molecular dynamics (MD) simulation study of the AchE-Q and AchE-Alb complexes provides in-depth insights into their structural stability, dynamics, and overall binding behavior over time. This analysis focuses on the Root Mean Square Deviation (RMSD), Root Mean Square Fluctuation (RMSF), and Radius of Gyration (Rg) of the protein-ligand complexes, which are key indicators of the stability, flexibility, and compactness of protein structures during the simulation.

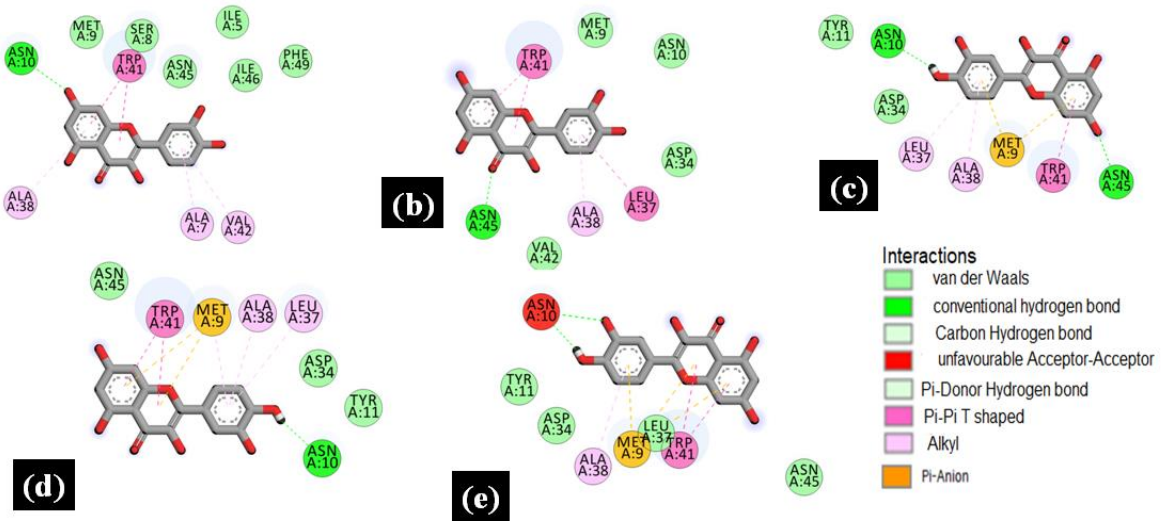

Figure 39. 2D display of binding interaction between Acetylcholinesterase and quercetins at (a) 10 ns (b) 20 ns, (c) 50 ns (d) 70 ns, and (d) 100 ns

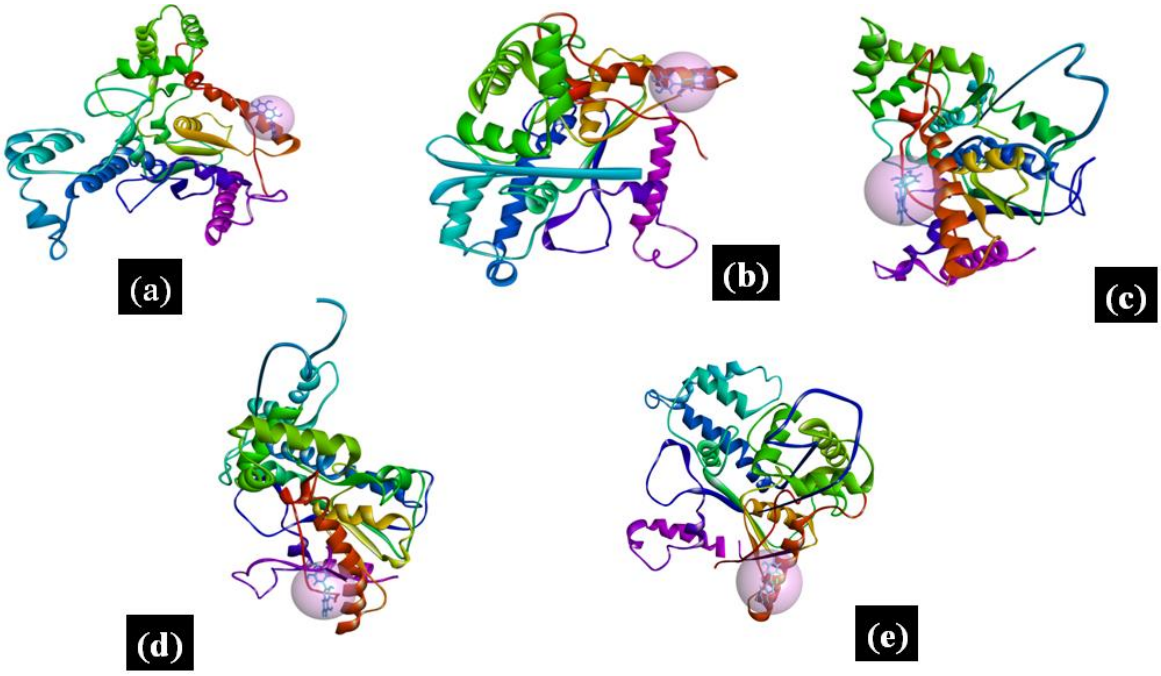

Figure 40. 3D display of binding interaction between AchE and quercetins at (a) 10 ns (b) 20 ns, (c) 50 ns (d) 70 ns, and (d) 100 ns

The RMSD values of both complexes were analyzed to assess the overall stability of the protein backbone during the simulation and shown in Figure 41a. The AchE-Q complex showed a relatively low average RMSD of 0.45, indicating that the complex remained quite stable and experienced minimal conformational changes over the simulation period. On the

other hand, the AchE-Alb complex exhibited a slightly higher average RMSD of 0.509, suggesting that this complex was subject to more structural fluctuations when compared to AchE-Q. Interestingly, the AchE-Q complex displayed a closer alignment to the Apo-protein with an average RMSD of 0.395, suggesting that the ligand binding in AchE-Q did not cause significant structural deviations from the native state of the protein. This could imply that the binding of Q to AchE stabilizes the complex in a conformation that is more closely related to the unbound protein (Apo-form).

In contrast, the AchE-Alb complex experienced a slight fluctuation at around 30 ns, where the RMSD increased to approximately 0.7. This rise in RMSD could indicate a temporary conformational adjustment or flexibility in the protein-ligand interface as the complex adapts to the binding of Alb. However, after this fluctuation, the complex stabilized, and the RMSD remained relatively constant till 100 ns. This suggests that, although the AchE-Alb complex displayed some initial flexibility, it eventually reached a stable configuration, with slightly more fluctuation compared to AchE-Q. This finding indicates that AchE-Q likely offers better binding stability, as evidenced by its more consistent RMSD throughout the simulation.

The RMSF analysis was conducted to examine the local flexibility of both complexes and shown in Figure 41b. This metric reveals how much each residue in the protein fluctuates from its average position during the simulation, which provides insights into the flexibility of different regions in the protein structure. The RMSF values for the Apo-protein, AchE-Q, and AchE-Alb were quite similar, with the Apo-protein exhibiting an average RMSF of 0.16, AchE-Alb showing an average of 0.17, and AchE-Q at 0.149. These values indicate that the flexibility profiles of both complexes were nearly identical to the Apo-protein, suggesting that the ligand binding did not induce significant changes in the overall flexibility of the proteins. However, the slight differences in RMSF values could indicate subtle shifts in the mobility of the protein's residues due to the specific interactions with the ligands. This is an important observation, as it suggests that while the protein maintains flexibility, it does so in a manner that doesn't greatly differ from the unbound state.

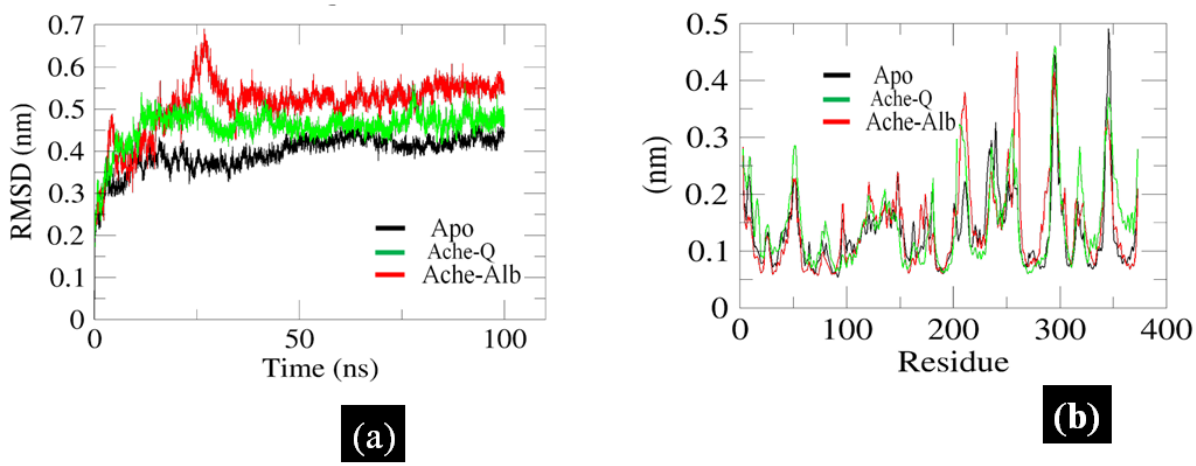

Figure 41. Conformational changes in the AchE complexes showing (a) RMSD of apo protein (AchE), AchE-Q and AchE-Alb with solvent, (b) RMS Fluctuation of amino acid residues

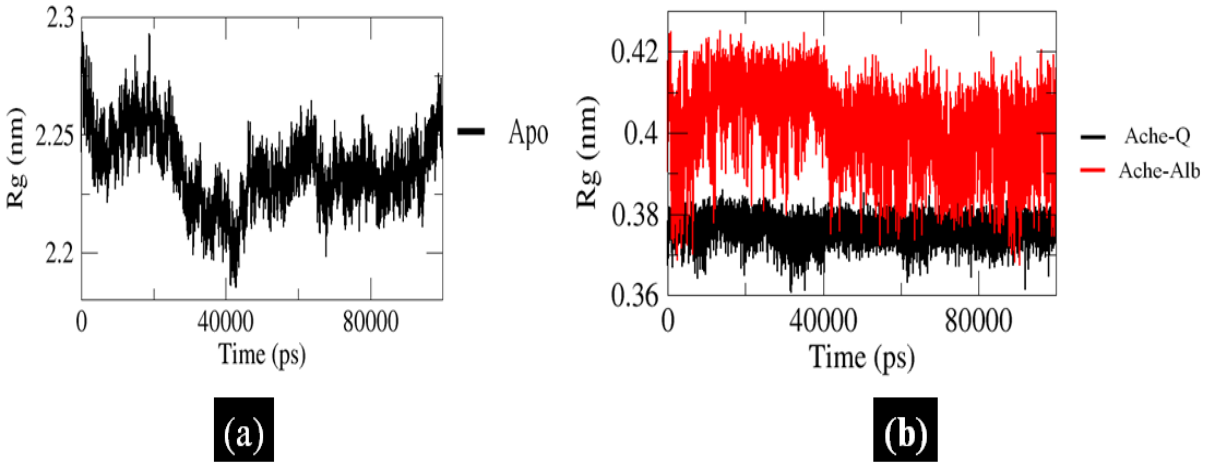

Figure 42. Radius of gyration of (a) AchE apo protein, and (b) Quercetin & albendazole-bound AchE complex, AchE = Acetylcholine esterase , Q = Quercetin, Alb = Albendazole, Apo-protein = AchE

The Rg is another important structural descriptor that helps measure the compactness of the protein or complex. Rg is particularly useful for understanding how the protein folds and whether it maintains its compact structure throughout the simulation. As shown in Figure 42, the AchE-Alb complex was found to be more compact than the AchE-Q complex, indicating that the AchE-Alb complex had a tighter, more compact conformation. This could be due to the specific binding interactions between AchE and Alb, which might promote a more compact structure through hydrophobic interactions and electrostatic forces. In comparison, the AchE-Q complex was slightly less compact, which might suggest that the interactions between AchE and Q do not induce as much compact packing

in the protein structure. Despite this difference, Rg analysis for both complexes and the Apo-protein revealed that all systems showed overall compact packing, indicating that the protein structures maintained their structural integrity throughout the simulation period. The results highlight that both complexes (AchE-Q and AchE-Alb) preserved their compactness and folding, which is essential for maintaining functional stability.

Figure 43a provides an in-depth analysis of the hydrogen bonds (H-bonds) involving the AchE-Q complex, AchE-Alb complex, and the apo-protein, particularly in the context of their interactions with the surrounding solvent. The results show that both the AchE-Q and AchE-Alb complexes formed a similar number of hydrogen bonds with the solvent, ranging from 700 to 850 bonds during the simulation. In contrast, the apo-protein exhibited a higher number of hydrogen bonds, ranging from over 800 to nearly 900 bonds. This suggests that the binding of Q and Alb to AchE may have led to a reduction in the protein's interaction with the solvent, resulting in fewer hydrogen bonds formed with water molecules. This decrease in H-bond formation with the solvent correlates with an increase in protein compactness. Specifically, the binding of the ligands might cause the protein structure to stabilize and compact, reducing its exposure to the surrounding solvent. The reduced number of H-bonds in the AchE-Q and AchE-Alb complexes when compared to the apo-protein highlights the structural impact of ligand binding. The ligands likely contribute to a more folded or compact structure, thereby decreasing the amount of solvent-accessible surface area for H-bonding.

Figure 43b provides further details on the hydrogen bonds formed between the ligands (Q and Alb) and the protein. The AchE-Alb complex exhibited up to 4 H-bonds with the ligand, while the AchE-Q complex formed 3 H-bonds during the simulation. These interactions were stable throughout the 100 ns period, indicating that the ligands remained strongly bound to the active site of the protein, with the hydrogen bonds playing a critical role in stabilizing the ligand-protein interaction. The AchE-Alb complex formed more hydrogen bonds with the ligand than AchE-Q, suggesting that Alb might engage in stronger or more stable interactions with AchE. This could reflect the different binding affinities or binding modes of the two ligands, which may have implications for their biological activities or therapeutic potential. Figure 44 also illustrates the total energy of the proteins throughout the 100 ns simulation, providing insights into the energy stability of the different complexes. Both the AchE-Q complex and the AchE-Alb complex showed nearly identical energy levels during the simulation, indicating that the ligand binding in both cases leads to similar stabilization of the protein structure. On the other hand, the apo-

protein exhibited higher energy levels compared to the complexes, suggesting that the unbound protein is in a less stable state. This higher energy could be indicative of a more flexible or less compact conformation of the apo-protein, which becomes more stable when bound to its respective ligands (Q or Alb). The energy comparison between the complexes and the apo-protein is important because it suggests that the binding of ligands not only influences the structural compactness (as seen in the RMSD and RMSF analyses) but also results in energy stabilization. Ligand binding might reduce the overall conformational flexibility of the protein, leading to lower energy states in the complexes, which is typically indicative of a more thermodynamically favorable state.

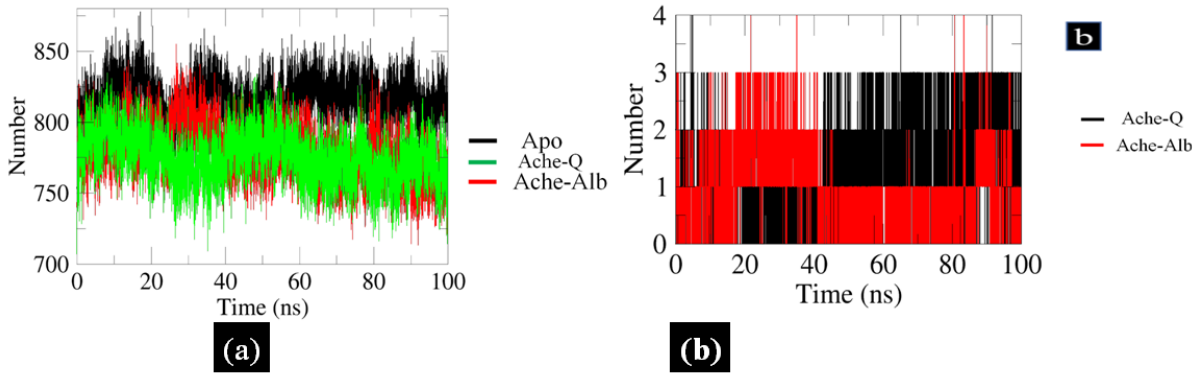

Figure 43. Confirmational changes in the AchE-quercetin complexes showing (a) total H bond between protein and solvent system, (b) H-bonds (HB) between quercetin and albendazole with AchEE protein. AchE = Acetylcholinesterase, Q = Quercetin, Alb= Albendazole, Apo-protein = ligand unbound AchE

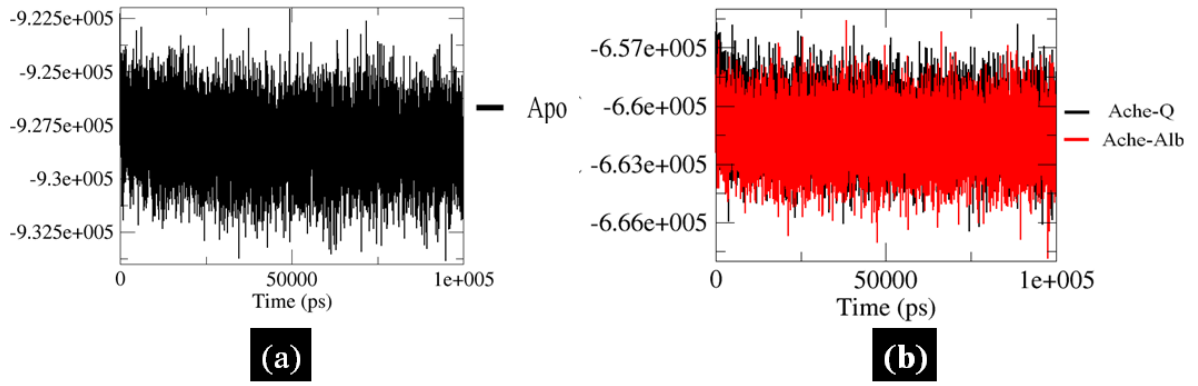

Figure 44. Total energy (-kJ/mol) of (a) AchE apo-protein, and (b) quercetin-bound AchE, and albendazole-bound AchE, AchE = Acetylcholinesterase, Q = Quercetin, Alb= Albendazole, Apo-protein = Ligand unbound AchE

4.20. MM/PBSA Analysis

Figure 45 presents the total binding energies and binding free energy changes for the AchE-Q and AchE-Alb complexes, providing a comprehensive view of the thermodynamic properties of these complexes. This analysis highlights the contributions of both the protein (receptor) and the ligand to the total binding energy and explores how these interactions contribute to the stability of the protein-ligand complex. The total binding energy of the complexes is primarily driven by two key interaction forces: (a) Van der Waals interactions and (b) Electrostatic interactions. These forces are essential in stabilizing the AchE-ligand complexes, as they facilitate close-range, non-covalent interactions between the protein and ligand. The Van der Waals energy contributes significantly to the binding process by promoting the optimal packing and close contact between non-polar regions of the ligand and the protein's hydrophobic surface. The electrostatic interactions help stabilize the protein-ligand complex through attraction between oppositely charged groups, further enhancing the binding affinity and overall stability.

As observed in the Figures, the AchE-Q complex displayed a more favorable binding energy compared to the AchE-Alb complex, which suggests that AchE-Q forms stronger and more stable interactions with the protein. The binding free energy changes (ΔG), which represent the thermodynamic favorability of ligand binding, were calculated and compared for both complexes. The AchE-Q complex showed a more favorable free energy change of -10.43 ± 4.31 kcal/mol, indicating that the binding of Q to AchE results in a thermodynamically more stable complex. This negative ΔG value suggests that the binding of Q is spontaneous and energetically favorable, which is a key indicator of its strong affinity for AchE. In contrast, the AchE-Alb complex exhibited a ΔG value of -8.69 ± 0.26 kcal/mol, which, although still negative, indicates that the binding of Alb to AchE is slightly less favorable compared to AchE-Q. The less negative free energy change suggests that the binding interaction between AchE and Alb is not as thermodynamically efficient as that of AchE-Q. These findings, displayed in Table 12, reflect the fact that AchE-Q has a stronger binding affinity and forms a more stable complex with AchE compared to AchE-Alb. The differences in ΔG values highlight the importance of ligand-structural interactions in determining the overall binding stability and thermodynamic favorability of the complex. The analysis of binding energy and binding free energy change (ΔG) demonstrates that the AchE-Q shows a more favorable thermodynamic profile, with a stronger binding affinity and more stable interactions with AchE. The binding energy is

primarily contributed by Van der Waals and electrostatic interactions, highlighting the importance of non-covalent forces in stabilizing protein-ligand complexes. The ΔG values indicate that AchE-Q binding is more spontaneous and energetically favorable compared to AchE-Alb. These thermodynamic properties provide critical insights into the binding mechanisms of AchE with its ligands, which could be crucial for understanding their potential biological activities and for drug design purposes, where stronger and more stable binding interactions are often desired.

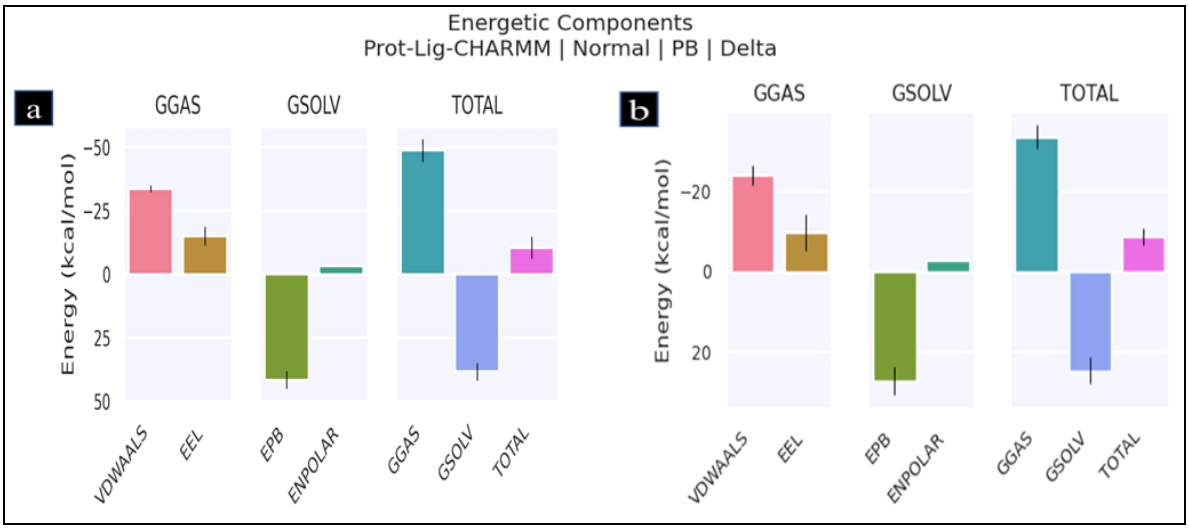

Figure 45. Free energy changes (Delta values) of protein complexes with (a) Quercetin and (b) Albendazole. All values are presented in kJ/mol

Table 8. Free energy changes (Delta values) of protein complexes (values are presented in kJ/mol)

Parameters	AchE-quercetin	AchE-albendazole
ΔVDWAALS	-33.67 ± 1.37	-23.87 ± 2.41
ΔEEL	-15.06 ± 3.66	-9.53 ± 4.58
ΔEPB	41.53 ± 3.56	27.41 ± 3.49
ΔENPOLAR	-3.24 ± 0.03	-2.71 ± 0.12
ΔGGAS	-48.73 ± 4.53	-33.39 ± 2.91
ΔSOLV	38.3 ± 3.57	24.70 ± 3.42
TOTAL	-10.43 ± 4.31	-8.69 ± 0.26

Values are expressed as mean ± SD

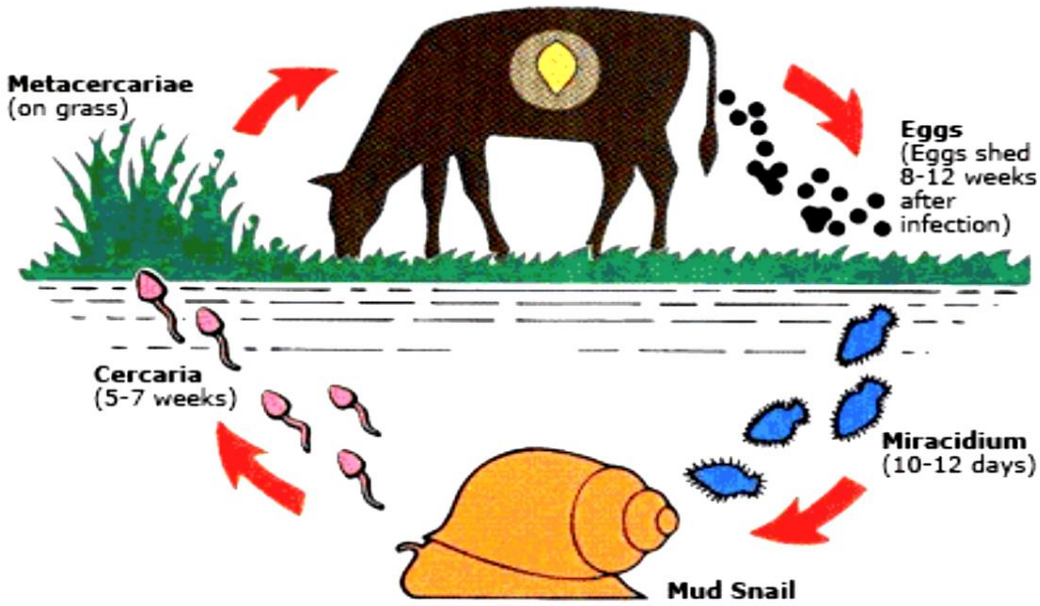

Photo plate 1. Life Cycle of Paramphistomum species along with the photos of the species

H. japonicum

Drying

Powder

Soaking

Crude extract

Rotary evaporator

Filtration

Photo plate 2. Preparation of methanolic extract of *Hypericum japonicum*

Solvent fractionation using separating funnel

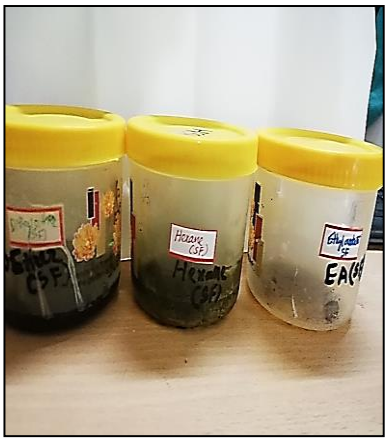

Solvent fractions

Photo plate 3. Solvent fractionation of plant extract of *Hypericum japonicum*

Photo plate 4. Treatment of helminth parasite with solvent fractions of *Hypericum japonicum*

Alkaloids

Tannins

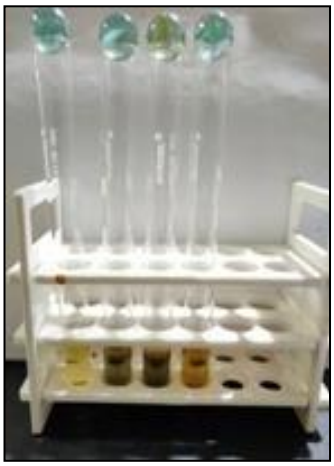

Phenols

Quinones

Terpenoids

Flavonoids

Coumarins

Anthrocyanins

Glycosides

Photo plate 5. Qualitative analysis of phytocompounds in solvent fractions of *Hypericum japonicum*. All the test tubes are in order: Hexane, Diethyl ether, Ethyl acetate and Methanol (From left to Right)

Anthraquinones

Steroids

Saponins

Proteins

Phlobatannins

Carbohydrates

Photo plate 6. Qualitative analysis of phytocompounds in solvent fractions of *Hypericum japonicum*. All the test tubes are in order: Hexane, Diethyl ether, Ethyl acetate and Methanol (From left to right)

(a) **(b)** **(c)** **(d)** **(e)**

Photo plate 7. Separation of phytocompounds in Thin Layer Chromatography using different solvent system. Slide size: 7.5 x 2.5 cm

(a) Petroleum ether : Ethyl acetate (3:1, v/v)

(b) Petroleum ether : Ethyl acetate (2:1, v/v)

(c) Petroleum ether : Ethyl acetate (1:2, v/v)

(d) Petroleum ether : Ethyl acetate (1:1, v/v)

(e) Petroleum ether : Ethyl acetate (1:3, v/v)

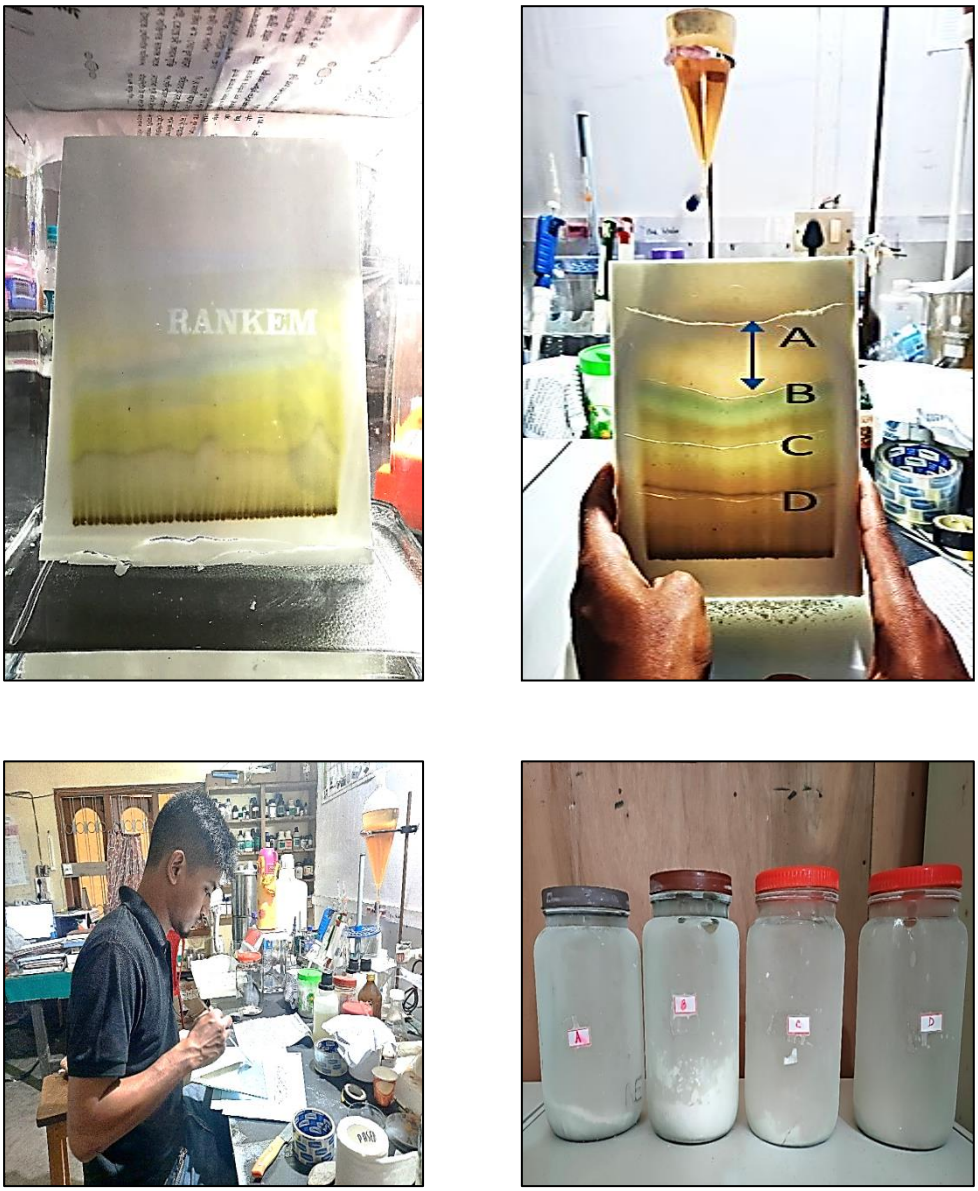

Photo plate 8. Separation of phytocompounds using larger TLC. Slide size: 21x17 cm (HxB), Solvent system: *Petroleum ether: Ethyl acetate (1:1, v/v)*